scientific reports

Check for updates

OPEN

A novel fractal fractional mathematical model for HIV/AIDS transmission stability and sensitivity with numerical analysis

Mukhtiar Khan[1,2], Nadeem Khan[3]✉, Ibad Ullah[4], Kamal Shah[4,5], Thabet Abdeljawad[5,6,7,8,9]✉ & Bahaaeldin Abdalla[5]

Understanding the complex dynamics of HIV/AIDS transmission requires models that capture real-world progression and intervention impacts. This study introduces an innovative mathematical framework using fractal-fractional calculus to analyze HIV/AIDS dynamics, emphasizing memory effects and nonlocal interactions critical to disease spread. By dividing populations into four distinct compartments-susceptible individuals, infected individuals, those undergoing treatment, and individuals in advanced AIDS stages-the model reflects key phases of infection and therapeutic interventions. Unlike conventional approaches, the proposed nonlinear transmission function, $\frac{\nabla(\mathscr{I}+\alpha_1\mathscr{T}+\alpha_2\mathscr{A})}{\mathscr{N}}$, accounts for varying infectivity levels across stages (where $\mathscr{N}$ is the total population and ∇ denotes the effective contact rate), offering a nuanced view of how treatment efficacy (α_1) and progression to AIDS (α_2) shape transmission. The analytical framework combines rigorous mathematical exploration with practical insights. We derive the basic reproduction number $\mathscr{R}_0$ to assess outbreak potential and employ Lyapunov theory to establish global stability conditions. Using the Schauder fixed-point theorem, we prove the existence and uniqueness of solutions, while bifurcation analysis via center manifold theory reveals critical thresholds for disease persistence or elimination. We use a computational scheme that combines the Adams-Bashforth method with an interpolation-based correction technique to ensure numerical precision and confirm theoretical results. Sensitivity analysis highlights medication accessibility and delaying the spread of AIDS as a vital control strategy by identifying (α_1) and (α_2) as critical parameters. The numerical simulations illustrate the predictive ability of the model, which shows how fractal-fractional order affects outbreak trajectories and long-term disease burden. The framework outperforms conventional integer order models and produces more accurate epidemiological predictions by integrating memory-dependent transmission with fractional order flexibility. These findings demonstrate the model's value in developing targeted public health initiatives, particularly in environments with limited resources where disease monitoring and balancing treatment allocation is essential. In the end, our work provides a tool to better predict and manage the evolving challenges of HIV/AIDS by bridging the gap between theoretical mathematics and actual disease control.

Keywords Fractal-Fractional Derivatives, Nonlinear Transmission, Memory Dependent Dynamics, Lyapunov Stability, Fixed Point Theorem

[1]College of Electrical Engineering and Computer Science, National Taiwan University, Taipei City 10617, Taiwan. [2]Research Center for Information Technology Innovation, Academia Sinica, Taipei 115201, Taiwan. [3]School of Automation, Central South University, Changsha, Hunan 410083, PR China. [4]Department of Mathematics, University of Malakand, Chakdara 18000, Khyber Pakhtunkhwa, Pakistan. [5]Department of Mathematics and Sciences, Prince Sultan University, Riyadh 11586, Saudi Arabia. [6]Department of Mathematics, Saveetha School of Engineering, Saveetha Institute of Medical and Technical Sciences, Saveetha University, Chennai, Tamil Nadu 602105, India. [7]Department of Mathematics, Kyung Hee University, 26 Kyungheedae ro, Dongdaemun-qu, Seoul, Republic of Korea. [8]Department of Mathematics and Applied Mathematics, School of Science and Technology, Sefako Makgatho Health Sciences University, Ga-Rankuwa, South Africa. [9]Department of Medical Research, China Medical University, Taichung 40402, Taiwan. ✉email: nadeemuom3@gmail.com; tabdeljawad@psu.edu.sa

One of the most persistent public health emergencies in the world, HIV (human immunodeficiency virus) continues to destroy millions of lives annually across the world before reaching its most severe form, known as AIDS (acquired immunodeficiency syndrome). The virus primarily weak the immune system by targeting $CD4+T$ cells, which are essential for protecting the body against infections[1,2]. In the absence of effective treatment, the depletion of these cells progressively impairs immune function, increasing susceptibility to opportunistic infections and specific types of cancer[3]. The most advanced stage of HIV infection, known as AIDS, is characterized by severe immune system failure. The virus is primarily transmitted through unprotected sexual contact, sharing infected needles, or from mother to child during childbirth or breastfeeding. Less commonly, transmission may occur through transfusion of infected blood or blood products. Certain demographic groups, such as men who have sex with men, individuals who inject drugs, commercial sex workers, and populations residing in regions with high HIV prevalence, exhibit an elevated risk of acquiring the virus[4–6]. During Human Immunodeficiency Virus (HIV) infection human bodies enter distinct stages beginning with acute infection and moving onto clinical latency before developing AIDS. The duration of HIV development between people differs widely according to individual cases and treatment-free infection spans multiple years to exceed one decade[7–9]. The medical community developed antiretroviral therapy (ART) as a breakthrough treatment which enabled clinicians to control HIV infection as a chronic manageable disease[10]. The combination of ART allows patients to achieve viral suppression that prevents further AIDS progression and reduces transmission probabilities to negligible levels. Regular use of ART gives people with HIV the opportunity to extend their lifespan while maintaining a healthy quality of life[11]. HIV/AIDS continues to affect people globally at substantial levels despite recent treatment developments. In 2023, 39.9 million people worldwide maintained an HIV diagnosis and 1.3 million new infections combined with 630, 000 AIDS-related fatalities were reported that year[12,13]. While East and Southern Africa, as well as parts of Eastern Europe and Central Asia, are disproportionately affected, young women and girls are at the highest risk of infection[14,15]. The global epidemic needs expanded preventive and treatment programs with equal funding levels and region-specific marketing initiatives to reduce its impact on populations[16]. Approximately sixty-seven percent of people living with HIV worldwide are found in Sub-Saharan Africa where the epidemic maintains its position as the epicenter[17]. Young women and girls face the greatest danger of acquiring HIV infections within East and Southern Africa together with Eastern European and Central Asian territories according to studies by the authors[18]. The global progress toward preventing and treating HIV has resulted in dropping infection numbers in various regions but unequal healthcare availability and ineffective outreach efforts persist to sustain inequality. Public health organizations must fight the epidemic through equal funding and personalized prevention programs and dynamic treatment solutions because failure to do so will worsen the damage[16].

Modern society depends on mathematical modeling to evaluate HIV transmission patterns and testing interventions because of its necessity[15,18,19]. The tools monitor disease spread patterns to assess treatment results for developing appropriate resource distribution plans. Public health policies undergo evaluation through modeling which uses transmission rates and patient medication adherence and behavioral change factors to predict long-term patterns and policy outcomes[16,20,21].

The models contribute to epidemic forecasting which speeds up targeted responses to diseases[22,23]. Traditional epidemic models underestimate real-life dynamics because they omit essential factors including previous disease spread influence on new infections and regional transmission differences[24–26]. The application of fractional-order models proves advantageous in such circumstances. The models exhibit biological memory and population healthcare differences through their analysis of extended spatial communication and location-independent phenomena[27–29]. Fractal calculus through fractional-order approaches detects transmission non-standard events that standard models fail to identify including sudden population increases in rural areas as well as urban hotspots[30–33]. The integrated approach leads to a flexible prediction system applicable to both epidemic control and medical care planning.

HIV/AIDS transmission behavior alongside therapy effects can be studied more accurately through the fractal-fractional method because this methodology incorporates processes beyond the scope of integer-order models. This framework considers how memory particles affect heterogeneity and non-local interactions to advance HIV/AIDS studies. The research findings enhance simulation accuracy and disease behavior understanding through better predictions[27,29].

Our research brings Atangana-Baleanu Caputo (ABC) operators to the present study because these operators form a cutting-edge mathematical framework for memory-based modeling. ABC operators differ from former fractional models through their application of Mittag-Leffler kernels which better describe HIV time evolution than traditional approaches according to references[34,35]. The use of ABC operators helps us resolve areas where previous studies lack clarity regarding past infections and treatment delays and accessibility issues. Fractional mathematics with fractal components in our model helps investigate how different population densities affect HIV transmission between cities and rural areas as well as the elevated risk patterns among specific demographic groups such as young women[36]. Researchers find these results essential to create practical interventions because they show how expanding access to antiretroviral medication (ART) and developing tailored prevention strategies for high-risk groups[37,38]. The assessment of potential intervention results can be achieved through scenario-based simulations in order to direct resources toward the most effective life-saving solutions[39,40].

The structure of the paper is organized as follows: Section "**Theory of Fractional Calculus**", presents the foundational principles and key concepts related to the Atangana-Baleanu fractional operator. In Section "**Fractional Order Model Formulation**", a mathematical model to analyze the transmission dynamics of HIV/AIDS, incorporating the memory effect and disease progression. The stability analysis of the model is thoroughly examined in Section " **Analysis of the Model**", while Section "**Fractional Dynamics Solution**" explores the existence and uniqueness of of the solution. In Section "**Fractional Dynamics via Adams-Bashforth Method**"

demonstrates the numerical iterations and computational approach. Finally, Section "**Conclusion**" outline the implications and suggests potential directions for future research.

Preliminaries

This section provides an overview of fundamental definitions and essential results that serve as the foundation for the subsequent analysis.

Definition 1 [29,41] The fractal-fractional derivative in the Atangana-Baleanu Caputo (ABC) sense, of fractional order $a \in (0,1]$ and fractal order $1 > b > 0$, for a function $\mathscr{G} \in C[0,T]$, is defined as:

$$ {}_0^{ABC}\mathscr{D}_t^{a,b}(\mathscr{G}(t)) = \frac{\mathscr{B}(a)}{1-a}\frac{d}{bt^{b-1}dt}\int_0^t E_a\left[-a\frac{(t-\tau)^a}{1-a}\right]\mathscr{G}(\psi)d\psi. \tag{1} $$

Here, $\mathscr{B}(a)$ is a normalization constant, $E_a(\cdot)$ represents the Mittag-Leffler function, and $\frac{d}{bt^{b-1}dt}$ denotes the fractional derivative in fractal order b. The choice of fractional order $a \in (0,1]$ reflects the non-local memory effects characteristic of many real-world systems, particularly in modeling complex biological and physical processes. When $a = 1$, the derivative reduces to the classical integer-order case, while smaller values of a capture long-term memory effects. The fractal order b accounts for the underlying fractal nature of the system. Many biological and epidemiological processes (such as disease spread on heterogeneous contact networks) exhibit fractal properties, where interactions occur across different scales. The parameter b adjusts the differential operator to accommodate the fractal dimension of the system. When $b = 1$, the derivative behaves as in standard fractional calculus, while lower values introduce additional scaling effects, allowing for more accurate modeling of complex dynamics.

For $\mathscr{G} \in L[0,T]$, the fractal-fractional integral in the Atangana-Baleanu Caputo sense, with fractional order $a \in (0,1]$ is defined as:

$$ {}_0^{ABC}I_t^{a,b}(\mathscr{G}(t)) = \frac{(1-a)bt^{b-1}}{\mathscr{B}(a)}\mathscr{G}(t) + \frac{ab}{\Gamma(a)\mathscr{B}(a)}\int_0^t \psi^{b-1}(t-\psi)^{a-1}\mathscr{G}(\psi)d\psi, \tag{2} $$

where $\Gamma(a)$ is the Gamma function, and the terms capture the memory-dependent and non-local nature of the operator. The function $\mathscr{B}(a)$ is a normalization function given by:

$$ \mathscr{B}(a) = 1 - a + \frac{a}{\Gamma(a)}. $$

The significance of using both fractional and fractal orders lies in their ability to model systems with complex structures and long-range dependencies, making them suitable for real-world applications such as disease modeling, diffusion processes, and anomalous transport phenomena.

Definition 2 [36,41] The *ABC* derivative exhibits Mittag-Leffler memory, expressed through the Mittag-Leffler function with index *a*, defined as:

$$ \mathscr{B}_a(t) = \sum_{j=0}^{\infty}\frac{t^j}{\Gamma(aj+1)}, \qquad a > 0. \tag{3} $$

Definition 3 [42] The effective contact rate (σ) is the average number of transmission-enabling contacts per unit time. It depends on treatment (e.g., ART reducing infectiousness), prevention and demographic factors (migration, birth, mortality). Thus, σ is dynamic and varies with epidemiological conditions and interventions.

Lemma 1 [43] Suppose $h \in L[0,T]$ and $h(0) = 0$, at $t = 0$. The solution of

$$ {}_0^{ABC}\mathscr{D}_t^{a,b}(\mathscr{G}(t)) = h(t), \quad \mathscr{G}(0) = G_0, $$

is given by:

$$ \mathscr{G}(t) = \mathscr{G}_0 + \frac{(1-a)bt^{b-1}}{\mathscr{B}(a)}h(t) + \frac{ab}{\Gamma(a)\mathscr{B}(a)}\int_0^t \psi^{b-1}(t-\psi)^{a-1}h(\psi)d\psi. \tag{4} $$

Main results

This section presents the principal findings of our study, highlighting their significance and relevance to the underlying problem.

Model formulation

The transmission pathway equation, $\frac{\nabla(\mathscr{I}+\alpha_1\mathscr{T}+\alpha_2\mathscr{A})}{\mathscr{N}}$, This equation describes the path through which $\mathscr{S}$ population members get infected. The variable $\mathscr{I}$ represents untreated infected persons while $\mathscr{T}$ stands for ART recipients and $\mathscr{A}$ consists of those at the advanced stage of AIDS. The values of α_1 and α_2 control how much

treated persons and people in advanced stages impact disease transmission because ART minimizes but does not completely remove infectivity. The total population ($\mathscr{N}$) acts as a normalization factor and ∇ represents the time-dependent rate of infectious pressure change. The population contains four primary compartments for HIV/AIDS progression including susceptible individuals ($\mathscr{S}$) and infected individuals ($\mathscr{I}$) as well as treated individuals ($\mathscr{T}$) and individuals in an advanced AIDS stage ($\mathscr{A}$) according to studies by[44,45]. The **Susceptible** ($\mathscr{S}$) those without HIV infection but at risk of exposure. Persons with HIV who have not started antiretroviral therapy (ART) comprise the **Infected** ($\mathscr{I}$) group. The **Treated** ($\mathscr{T}$) Under antiretroviral therapy (ART) patients achieve near undetectable viral levels thus reducing HIV disease advancement while eliminating the possibility of virus spread. People with advanced disease status ($\mathscr{A}$) classified as AIDS represent the last group in the HIV disease stages while their transmission levels depend on their treatment adherence.

Thorough analysis of these population subgroups enables thorough understanding of HIV/AIDS evolution and its management processes. Preventive measures such as education campaigns and pre-exposure prophylaxis (PrEP) maintain high importance in reducing new infections according to the susceptible cohort ($\mathscr{S}$). The timely diagnosis and quick referral to care represents a critical necessity for patients in the infected group because untreated patients propagate the infection because of increased viral load levels. Sustained antiretroviral therapy (ART) by the treated cohort ($\mathscr{T}$) reduces viral replication rates which breaks transmission chains and leads to life expectancy improvement. Studies of AIDS patients who delayed treatment access demonstrate that advanced immunosuppression raises mortality chances yet palliative ART maintains stabilized health results regardless of disease progression[46–48]. Among the proposed fractal-fractional models depicted in Fig. 1 stands one that integrates both memory effects and non-local dynamics of HIV/AIDS transmission through Atangana-Baleanu operators. The new framework achieves both treatment representation accuracy by considering platform delays and varied transmission patterns as well as operational efficiency allowing policymakers to conduct modeling analyses involving prevention measures or treatment implementation delays. This mathematical model generates useful guidance for testing campaign strategies and treatment access decisions and resource allocation determination in regions with high HIV/AIDS burdens by creating a strong link between theoretical rigor and observed epidemiological events[49,50].

The model equations are given by:

$$\begin{cases} {}^{\mathscr{FFM}}\mathscr{D}_t^{a,b}\mathscr{S}(t) = \nabla - \sigma\left(\frac{\mathscr{I}+\alpha_1\mathscr{T}+\alpha_2\mathscr{A}}{\mathscr{N}}\right)\mathscr{S} - \eta\mathscr{S}, \\ {}^{\mathscr{FFM}}\mathscr{D}_t^{a,b}\mathscr{I}(t) = \sigma\left(\frac{\mathscr{I}+\alpha_1\mathscr{T}+\alpha_2\mathscr{A}}{\mathscr{N}}\right)\mathscr{S} - (\eta+\beta_1+\zeta_1)\mathscr{I}, \\ {}^{\mathscr{FFM}}\mathscr{D}_t^{a,b}\mathscr{A}(t) = \zeta_1\mathscr{I} + \varrho\mathscr{T} - (\gamma_1+\lambda_1+\eta)\mathscr{A}, \\ {}^{\mathscr{FFM}}\mathscr{D}_t^{a,b}\mathscr{T}(t) = \beta_1\mathscr{I} + \gamma_1\mathscr{A} - (\eta+\varrho)\mathscr{T}. \end{cases} \tag{5}$$

The initial conditions are:

$$\mathscr{S}(0) = \mathscr{S}_0 \geq 0, \quad \mathscr{I}(0) = \mathscr{I}_0 \geq 0, \quad \mathscr{A}(0) = \mathscr{A}_0 \geq 0, \quad \mathscr{T}(0) = \mathscr{T}_0 \geq 0.$$

To simplify computations, we define:

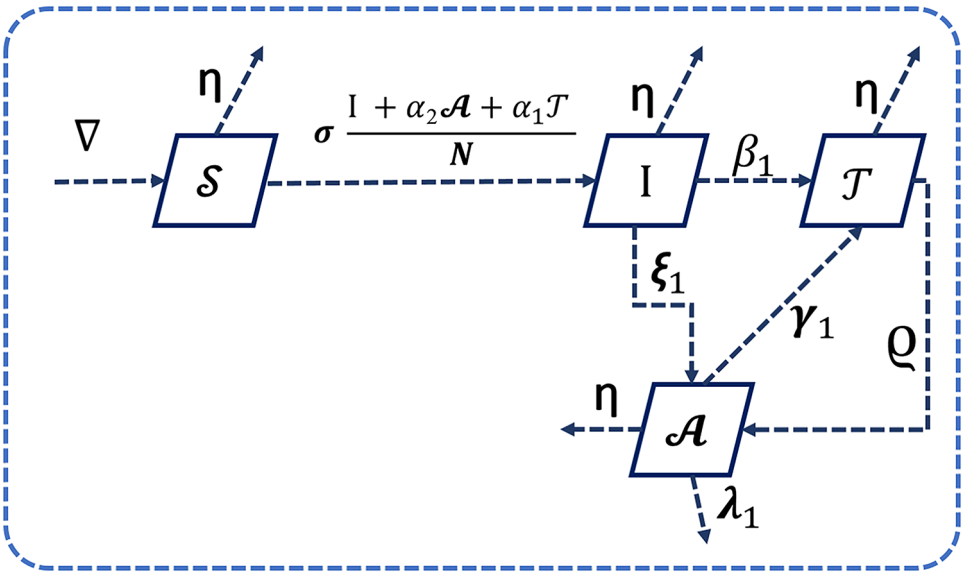

Fig. 1. HIV/AIDS compartmental model structure, depicting transitions between susceptible (*S*), infected (*I*), treated (*T*), and advanced-stage (*A*) populations. The fractal-fractional framework with Atangana-Baleanu operators integrates memory dependent transmission, spatial heterogeneity, and treatment effects to evaluate intervention impacts on epidemic dynamics.

$$\kappa = \sigma\left(\frac{\mathscr{I} + \alpha_1\mathscr{T} + \alpha_2\mathscr{A}}{\mathscr{N}}\right), \quad m_1 = \eta + \beta_1 + \zeta_1, \quad m_2 = \gamma_1 + \lambda_1 + \eta, \quad m_3 = \eta + \varrho.$$

Substituting these into (5), the system is rewritten as:

$$\begin{cases} {}^{\mathscr{FFM}}\mathscr{D}_t^{a,b}\mathscr{S}(t) = \nabla - \kappa(t)\mathscr{S} - \eta\mathscr{S}, \\ {}^{\mathscr{FFM}}\mathscr{D}_t^{a,b}\mathscr{I}(t) = \kappa(t)\mathscr{S} - m_1\mathscr{I}, \\ {}^{\mathscr{FFM}}\mathscr{D}_t^{a,b}\mathscr{A}(t) = \zeta_1\mathscr{I} + \varrho\mathscr{T} - m_2\mathscr{A}, \\ {}^{\mathscr{FFM}}\mathscr{D}_t^{a,b}\mathscr{T}(t) = \beta_1\mathscr{I} + \gamma_1\mathscr{A} - m_3\mathscr{T}. \end{cases} \tag{6}$$

The parameters are defined in Table 1.

Fundamental characteristics of the model

This subsection investigates the core mathematical characteristics of the Atangana-Baleanu HIV/AIDS epidemic model[31,51]. The analysis emphasizes the existence, uniqueness, and positivity of the solutions, which are essential for the model's applicability to real-world scenarios. Define:

$$\mathbb{R}_+^4 = \{x \in \mathbb{R}^4 \mid x \geq 0\}, \quad x(t) = (\mathscr{S}(t), \mathscr{I}(t), \mathscr{A}(t), \mathscr{T}(t))^T.$$

The generalized mean value theorem, as described in[38,52], is formally stated as follows:

Lemma 2 *Let* $\mathscr{H}(x) \in C[a_1, a_2]$ *and* ${}^{\mathscr{FFM}}\mathscr{D}_t^{a,b}\mathscr{H}(x) \in (a_1, a_2]$. *Then:*

$$\mathscr{H}(t) = \mathscr{H}(a_1) + \frac{1}{\Gamma(a,b)}\left({}^{\mathscr{FFM}}\mathscr{D}_t^{a,b}\mathscr{H}(\mathscr{Y})(t - a_1)^{a,b}\right),$$

where $a_1 \leq \mathscr{Y} \leq t, \forall t \in (a_1, a_2]$.

Corollary 1 [53] *Suppose* $\mathscr{H}(x) \in C[a_1, a_2]$ *and* ${}^{\mathscr{FFM}}\mathscr{D}_t^{a,b}\mathscr{H}(x) \in C[a_1, a_2]$, *where* $a, b \in (0, 1]$. *Then:*

- If ${}^{\mathscr{FFM}}\mathscr{D}_t^{a,b}\mathscr{H}(x) \geq 0, \forall x \in (a_1, a_2)$, $\mathscr{H}$ *is non-decreasing.*
- If ${}^{\mathscr{FFM}}\mathscr{D}_t^{a,b}\mathscr{H}(x) \leq 0, \forall x \in (a_1, a_2)$, $\mathscr{H}$ *is non-increasing.*

Theorem 1 *A unique solution* $x(t)$ *to the system* (5) *exists and remains confined within the positive cone* $\mathbb{R}_+^4$. *Moreover, the solution maintains positivity for all* $t \geq 0$.

Proof The existence of solutions follows from Theorem 3.1 in[23,54], and uniqueness is guaranteed by Remark 3.2 in[54,55] for $t > 0$. To ensure positivity, the vector field must point inward on the boundaries of the non-negative orthant. Evaluating system (6) on these boundaries:

$$\begin{cases} {}^{\mathscr{FFM}}\mathscr{D}_t^{a,b}\mathscr{S}(t)\Big|_{\mathscr{S}=0} = \nabla \geq 0, \\ {}^{\mathscr{FFM}}\mathscr{D}_t^{a,b}\mathscr{I}(t)\Big|_{\mathscr{I}=0} = \sigma\kappa(t)\mathscr{S} \geq 0, \\ {}^{\mathscr{FFM}}\mathscr{D}_t^{a,b}\mathscr{A}(t)\Big|_{\mathscr{A}=0} = \zeta_1\mathscr{I} + \varrho\mathscr{T} \geq 0, \\ {}^{\mathscr{FFM}}\mathscr{D}_t^{a,b}\mathscr{T}(t)\Big|_{\mathscr{T}=0} = \beta_1\mathscr{I} + \gamma_1\mathscr{A} \geq 0. \end{cases} \tag{7}$$

To justify why $\zeta_1\mathscr{I} + \varrho\mathscr{T} \geq 0$, we note that ζ_1 and ϱ are non-negative parameters representing transition rates between compartments, and $\mathscr{I}, \mathscr{T}$ are population variables, which are inherently non-negative due to

Symbol	Physical Interpretation
∇	Recruitment rate of $\mathscr{S}(t)$
α_1	Modification parameter for the treatment class
α_2	Modification parameter for the AIDS class
η	Natural death rate
β_1	Infection rate
λ_1	Death rate due to AIDS
ϱ	Fraction of improperly buried individuals
ζ_1	Progression rate from the infected to AIDS class
σ	Effective contact rate
γ_1	Progression rate from the treatment to AIDS class

Table 1. Key symbols and their corresponding physical interpretations in the HIV/AIDS model (5).

their biological meaning. Since these terms represent contributions to the $\mathscr{A}$-compartment, they must be non-negative to ensure a physically meaningful model.

Hence, solutions remain in $\mathbb{R}^4_+$ for $t \geq 0$. To show boundedness, summing the equations in (6) gives:

$$^{\mathscr{FFM}}\mathscr{D}_t^{a,b}\mathscr{N}(t) = \nabla - \eta\mathscr{N}(t) - \eta_1\mathscr{T}(t), \tag{8}$$

where

$$^{\mathscr{FFM}}\mathscr{D}_t^{a,b}\mathscr{N}(t) \leq \nabla - \eta\mathscr{N}(t). \tag{9}$$

Solving this inequality:

$$\lim_{t\to\infty} \sup \mathscr{N}(t) \leq \frac{\nabla}{\eta}. \tag{10}$$

Thus, the biologically feasible region is defined as:

$$\Phi = \left\{(\mathscr{S}, \mathscr{I}, \mathscr{A}, \mathscr{T}) \in \mathbb{R}^4_+ : \mathscr{S}, \mathscr{I}, \mathscr{A}, \mathscr{T} \geq 0, \mathscr{N} \leq \frac{\nabla}{\eta}\right\}. \tag{11}$$

□

The next subsection examines the equilibria and the basic reproduction number $\mathscr{R}_0$.

Steady-state analysis and the basic reproduction number ($\mathscr{R}_0$)

This section is further divided in to some sub sections.

Equilibrium points and basic reproduction number $\mathscr{R}_0$

The proposed HIV/AIDS model, as formulated in Equation (5), exhibits two equilibrium states: the **disease-free equilibrium (DFE)** and the **endemic equilibrium (EE)**.

Disease-Free Equilibrium (DFE)

The disease-free equilibrium represents a scenario where no infection persists in the population. It is given by:

$$E_0 = \left\{\frac{\nabla}{\eta}, 0, 0, 0\right\},$$

where ∇ denotes the recruitment rate into the population, and η is the natural mortality rate. At this equilibrium, all individuals are susceptible, and there are no active infections.

Endemic Equilibrium (EE)

The endemic equilibrium E_1 represents the steady-state condition where the infection persists in the population. It is expressed as:

$$E_1 = \begin{cases} \mathscr{S}^* = \frac{\nabla}{\sigma\frac{\mathscr{I}^*+\alpha_1\mathscr{T}^*+\alpha_2\mathscr{A}^*}{\mathscr{N}^*}+\eta}, \\ \mathscr{I}^* = \frac{\mathscr{N}^*(\nabla-\eta(\eta+\beta_1+\zeta_1))}{\eta+\beta_1+\zeta_1+\alpha_1\mathscr{T}^*+\alpha_2\mathscr{A}^*}, \\ \mathscr{A}^* = \frac{\zeta_1\mathscr{I}^*+\varrho\mathscr{T}^*}{\gamma_1+\lambda_1+\eta}, \\ \mathscr{T}^* = \frac{\beta_1\mathscr{I}^*(\gamma_1+\lambda_1+\eta)+\gamma_1\zeta_1\mathscr{I}^*}{(\eta+\varrho)(\gamma_1+\lambda_1+\eta)-\gamma_1\varrho}. \end{cases} \tag{12}$$

At this equilibrium, all compartments of the population-susceptible ($\mathscr{S}$), infected ($\mathscr{I}$), treated ($\mathscr{T}$), and AIDS ($\mathscr{A}$)-have nonzero steady-state values, indicating the persistence of the infection under certain parameter conditions.

Basic reproduction number $\mathscr{R}_0$

The **basic reproduction number** $\mathscr{R}_0$ is a fundamental threshold parameter that determines whether an infection will spread or die out within a population. It represents the expected number of secondary infections generated by a single infected individual in a completely susceptible population. If $\mathscr{R}_0 < 1$, the disease is expected to die out, whereas if $\mathscr{R}_0 > 1$, the infection may persist and become endemic.

In this model, $\mathscr{R}_0$ is computed using the **Next-Generation Matrix (NGM) method**[56,57]. The method involves defining the matrices for new infections ($\mathscr{X}$) and transition rates ($\mathscr{Y}$) as follows:

$$\mathscr{X} = \begin{pmatrix} \sigma\frac{\mathscr{I}+\alpha_1\mathscr{T}+\alpha_2\mathscr{A}}{\mathscr{N}}\mathscr{S} \\ 0 \end{pmatrix}, \quad \mathscr{Y} = \begin{pmatrix} -(\eta+\beta_1+\zeta_1)\mathscr{I} \\ \zeta_1\mathscr{I}+\varrho\mathscr{T}-(\gamma_1+\lambda_1+\eta)\mathscr{A} \end{pmatrix}. \tag{13}$$

The Jacobian matrices evaluated at the disease-free equilibrium (DFE) are given by:

$$\mathscr{X}^* = \begin{pmatrix} \frac{\sigma\nabla}{\eta\mathscr{N}} & 0 \\ 0 & 0 \end{pmatrix}, \quad \mathscr{Y}^* = \begin{pmatrix} \eta+\beta_1+\zeta_1 & 0 \\ -\zeta_1 & \gamma_1+\lambda_1+\eta \end{pmatrix}. \tag{14}$$

The basic reproduction number is determined as the **spectral radius** of the matrix product $\mathscr{X}^*\mathscr{Y}^{*-1}$, yielding:

$$\mathscr{R}_0 = \varrho(\mathscr{X}^*\mathscr{Y}^{*-1}) = \frac{\sigma\nabla\left((\gamma_1+\lambda_1+\eta)+\alpha_1\zeta_1\right)}{\eta\mathscr{N}(\beta_1+\zeta_1+\eta)(\gamma_1+\lambda_1+\eta)}. \tag{15}$$

Sensitivity analysis of $\mathscr{R}_0$

Sensitivity analysis of the basic reproduction number ($\mathscr{R}_0$) is essential for identifying key parameters that influence disease transmission and control. This analysis quantifies the effect of parameter variations on $\mathscr{R}_0$ using the normalized sensitivity index[58,59]:

$$\mathscr{Q}_y^{\mathscr{R}_0} = \frac{y}{\mathscr{R}_0}\left[\frac{\partial\mathscr{R}_0}{\partial y}\right], \tag{16}$$

where $y \in \{\sigma, \nabla, \gamma_1, \lambda_1, \eta, \alpha_1, \zeta_1, \beta_1\}$.

The expression for $\mathscr{R}_0$ in this model is:

$$\mathscr{R}_0 = \frac{\sigma\nabla\left[(\gamma_1+\lambda_1+\eta)+\alpha_1\zeta_1\right]}{\eta\mathscr{N}(\beta_1+\zeta_1+\eta)(\gamma_1+\lambda_1+\eta)}. \tag{17}$$

Sensitivity indices for key parameters are derived as follows:

$$\begin{cases} \mathscr{Q}_\sigma = 1, \\ \mathscr{Q}_\nabla = 1, \\ \mathscr{Q}_{\alpha_1} = \frac{\zeta_1\alpha_1}{(\gamma_1+\lambda_1+\eta)\left(1+\frac{\alpha_1\zeta_1}{\gamma_1+\lambda_1+\eta}\right)}, \\ \mathscr{Q}_{\zeta_1} = \frac{\alpha_1\zeta_1}{(\gamma_1+\lambda_1+\eta)\left(1+\frac{\alpha_1\zeta_1}{\gamma_1+\lambda_1+\eta}\right)}, \\ \mathscr{Q}_{\gamma_1} = -\frac{\alpha_1\zeta_1\gamma_1}{(\gamma_1+\lambda_1+\eta)^2\left(1+\frac{\alpha_1\zeta_1}{\gamma_1+\lambda_1+\eta}\right)}, \\ \mathscr{Q}_{\lambda_1} = -\frac{\alpha_1\zeta_1\lambda_1}{(\gamma_1+\lambda_1+\eta)^2\left(1+\frac{\alpha_1\zeta_1}{\gamma_1+\lambda_1+\eta}\right)}, \\ \mathscr{Q}_\eta = -\frac{\left[(\gamma_1+\lambda_1+\eta)-\frac{\alpha_1\zeta_1}{(\gamma_1+\lambda_1+\eta)^2}\right]\eta}{\left(1+\frac{\alpha_1\zeta_1}{\gamma_1+\lambda_1+\eta}\right)}, \\ \mathscr{Q}_{\beta_1} = -\frac{\beta_1}{\beta_1+\zeta_1+\eta}. \end{cases} \tag{18}$$

In Fig. 2, we presented the sensitivity analysis graphically.

Figure 3 further illustrates the impact of key parameters on $\mathscr{R}_0$:

From Fig. 3, we observe:

- Higher σ increases $\mathscr{R}_0$, emphasizing the need for reducing contact rates and improving preventive measures.

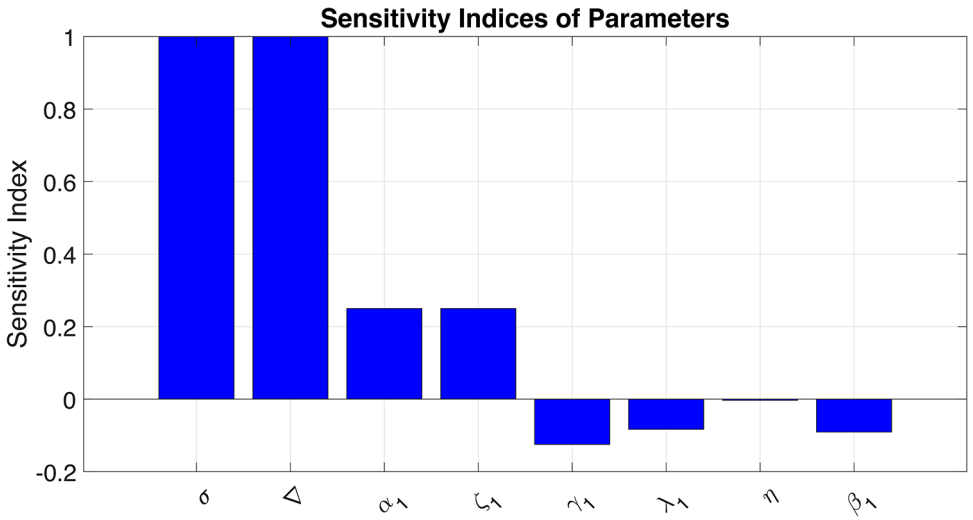

Fig. 2. Sensitivity indices of various parameters, highlighting their relative contributions to $\mathscr{R}_0$. Higher indices indicate greater influence on disease transmission.

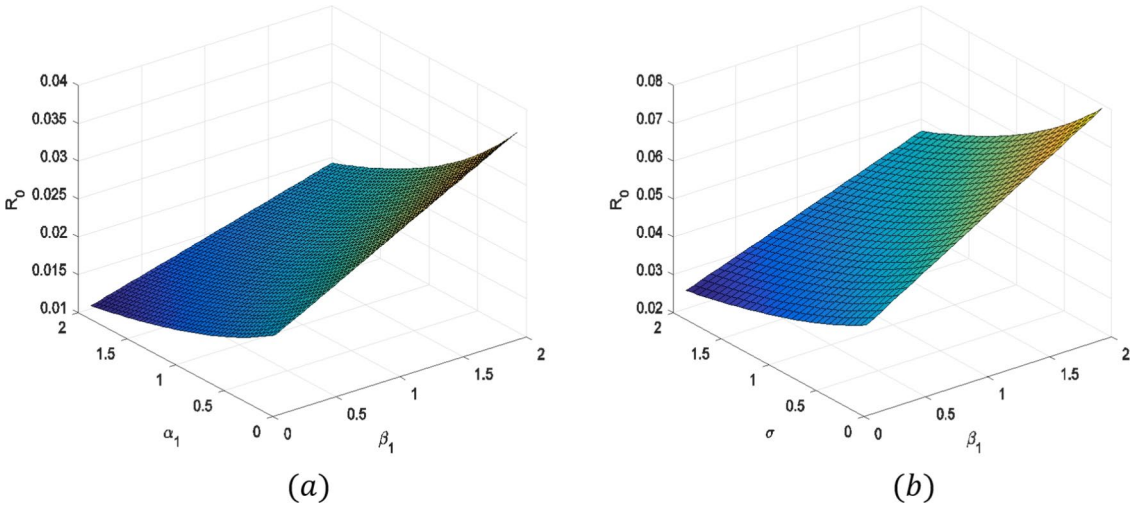

Fig. 3. Effects of different parameters on $\mathscr{R}_0$. The left panel (**a**) shows variation with respect to α_1 (progression rate) and β_1 (infection rate), while the right panel (**b**) illustrates the influence of σ (transmission rate) and β_1. Higher values of these parameters increase $\mathscr{R}_0$, suggesting a greater risk of disease persistence.

- Higher β_1 and α_1 lead to increased $\mathscr{R}_0$, highlighting the importance of timely treatment and behavioral interventions.
- The interaction between treatment effects (η) and progression rates (ζ_1) underscores the role of early intervention in reducing $\mathscr{R}_0$.

Incorporating **fractal-fractional operators** enhances traditional models by considering **memory effects, spatial heterogeneity, and anomalous diffusion**, providing a more accurate representation of HIV/AIDS dynamics. This approach is crucial for devising effective control strategies[23,55].

Stability analysis of the Disease-Free Equilibrium (DFE)

Local stability of the DFE

Theorem 2 *The system given by Equation (5) is locally asymptotically stable at the disease-free equilibrium (DFE), denoted as E_0, if the basic reproduction number satisfies $\mathscr{R}_0 < 1$. If $\mathscr{R}_0 > 1$, the equilibrium E_0 becomes unstable. Unlike integer-order systems, the stability of a fractional-order model depends not only on the eigenvalues of the Jacobian matrix but also on the fractional-order parameter, which influences memory effects and system dynamics.*

Proof For fractional-order differential equations, stability is determined by the argument of the eigenvalues rather than just their real parts, as in ordinary differential equations (ODEs). The system is locally asymptotically stable if all eigenvalues λ of the Jacobian matrix at E_0 satisfy:

$$|\arg(\lambda)| > \frac{a\pi}{2}, \tag{19}$$

where *a* is the fractional order of differentiation.

The Jacobian matrix at E_0 is:

$$J = \begin{pmatrix} -\eta & -\sigma & -\sigma\alpha_2 & -\sigma\alpha_1 \\ 0 & \sigma - (\zeta_1 + \beta_1 + \eta) & \sigma\alpha_2 & \sigma\alpha_1 \\ 0 & \zeta_1 & -(\gamma_1 + \lambda_1 + \eta) & \varrho \\ 0 & \beta_1 & \gamma_1 & -(\varrho + \eta) \end{pmatrix}. \tag{20}$$

One eigenvalue of *J* is $\lambda_1 = -\eta$. The reduced matrix J_1 for the remaining eigenvalues is:

$$J_1 = \begin{pmatrix} p_1 & \sigma\alpha_2 & \sigma\alpha_1 \\ \zeta_1 & -p_2 & \varrho \\ \beta_1 & \gamma_1 & -p_3 \end{pmatrix}, \tag{21}$$

where:

$$\begin{aligned} p_1 &= \sigma - (\zeta_1 + \beta_1 + \eta), \\ p_2 &= \gamma_1 + \lambda_1 + \eta, \\ p_3 &= \varrho + \eta. \end{aligned}$$

The characteristic equation is:

$$\lambda^3 + a_1\lambda^2 + a_2\lambda + a_3 = 0, \tag{22}$$

where the coefficients are:

$$\begin{aligned} a_1 &= p_2 + p_3 - p_1, \\ a_2 &= p_1p_2 + p_1p_3 + p_2p_3 - \varrho\gamma_1 - \sigma\alpha_2\zeta_1 - \sigma\alpha_1\beta_1, \\ a_3 &= p_1p_2p_3 - p_1\varrho\gamma_1 - \sigma\alpha_2\varrho\beta_1 - \sigma\alpha_1\zeta_1\gamma_1. \end{aligned}$$

For the fractional-order system, applying the Matignon criterion, stability requires that all eigenvalues satisfy:

$$|\arg(\lambda)| > \frac{a\pi}{2}, \quad \text{for } 0 < a \leq 1. \tag{23}$$

When $a = 1$, the fractional model reduces to an ODE system, and stability is determined using the standard Routh-Hurwitz conditions: $a_1 > 0$, $a_2 > 0$, $a_3 > 0$, and $(a_1a_2 - a_3)/a_1 > 0$. However, for $a < 1$, stability conditions depend on the memory effects introduced by the fractional derivative, leading to a broader range of dynamical behaviors compared to integer-order systems. □

Global stability of the DFE
Theorem 3 *The DFE, $\mathscr{E}_0$, is globally asymptotically stable if $\mathscr{R}_0 < 1$.*

Proof Define the Lyapunov function:

$$\mathscr{G}(t) = q_1\left(\mathscr{S} - \mathscr{S}^0 - \mathscr{S}^0\ln\left(\frac{\mathscr{S}}{\mathscr{S}^0}\right)\right) + q_2\mathscr{I} + q_3\mathscr{A} + q_4\mathscr{T}. \tag{24}$$

Taking its fractional derivative and substituting model equations, we obtain:

$${}^{\mathscr{F}\mathscr{F}\mathscr{M}}\mathscr{D}_t^{a,b}\mathscr{G}(t) = -\eta q_1\frac{(\mathscr{S}^0 - \mathscr{S})^2}{\mathscr{S}^0} + (\eta + \beta_1 + \zeta_1)(\mathscr{R}_0 - 1)\mathscr{I}.$$

For $\mathscr{R}_0 \leq 1$, ${}^{\mathscr{F}\mathscr{F}\mathscr{M}}\mathscr{D}_t^{a,b}\mathscr{G}(t) \leq 0$, with equality only at $\mathscr{E}_0$. By LaSalle's invariance principle, $\mathscr{E}_0$ is globally asymptotically stable. □

Global stability of the endemic equilibrium
Theorem 4 *The endemic equilibrium $\mathscr{E}_1 = (\mathscr{S}^*, \mathscr{I}^*, \mathscr{A}^*, \mathscr{T}^*)$ is globally asymptotically stable if $\mathscr{R}_0 > 1$.*

Proof Define the Lyapunov function:

$$\begin{aligned} \mathscr{L} = (\mathscr{S} - \mathscr{S}^*) + (\mathscr{I} - \mathscr{I}^*) + (\mathscr{A} - \mathscr{A}^*) + (\mathscr{T} - \mathscr{T}^*) \\ - (\mathscr{S}^* + \mathscr{I}^* + \mathscr{A}^* + \mathscr{T}^*) - \ln\left(\frac{\mathscr{S} + \mathscr{I} + \mathscr{A} + \mathscr{T}}{\mathscr{S}^* + \mathscr{I}^* + \mathscr{A}^* + \mathscr{T}^*}\right). \end{aligned}$$

Taking its fractional derivative and substituting equilibrium conditions, we obtain:

$${}^{\mathscr{F}\mathscr{F}\mathscr{M}}\mathscr{D}_t^{a,b}\mathscr{L}(t) = -\eta\frac{(\mathscr{S} + \mathscr{I} + \mathscr{A} + \mathscr{T} - (\mathscr{S}^* + \mathscr{I}^* + \mathscr{A}^* + \mathscr{T}^*))^2}{\mathscr{S} + \mathscr{I} + \mathscr{A} + \mathscr{T}} < 0.$$

Since $\mathscr{L}$ is positive definite and its derivative is negative definite, $\mathscr{E}_1$ is globally asymptotically stable by LaSalle's principle. □

Bifurcation analysis

Here, the possibility of the co-existence of the disease-free equilibrium and endemic equilibrium at $\mathscr{R}_0 < 1$ is explored using the center manifold theory[60,61] to investigate the occurrence of bifurcation in the presence of loss of immunity after recovery. The model (5) can be written in vector form ${}_0^{ABC}\mathscr{D}_t^{a,b}(\mathscr{Z}(t)) = F_1(z)$, where $\mathscr{Z} = (z_1, z_2, z_3, z_4)^T$ and $\mathscr{Z} = (f_1, f_2, f_3, f_4)^T$, such that $\mathscr{S} = z_1, \mathscr{I} = z_2, \mathscr{A} = z_3, \mathscr{T} = z_4$. Then, the HIV/AIDS model becomes:

$$\begin{cases} f_1 = {}_0^{ABC}\mathscr{D}_t^{a,b}\mathscr{Z}_1(t) = \nabla - \sigma\left(\frac{z_2 + \alpha_1z_4 + \alpha_2z_3}{\mathscr{N}}\right)z_1 - \eta z_1, \\ f_2 = {}_0^{ABC}\mathscr{D}_t^{a,b}\mathscr{Z}_2(t) = \sigma\left(\frac{z_2 + \alpha_1z_4 + \alpha_2z_3}{\mathscr{N}}\right)z_1 - (\eta + \beta_1 + \zeta_1)z_2, \\ f_3 = {}_0^{ABC}\mathscr{D}_t^{a,b}\mathscr{Z}_3(t) = \zeta_1z_2 + \varrho z_4 - (\gamma_1 + \lambda_1 + \eta)z_3, \\ f_4 = {}_0^{ABC}\mathscr{D}_t^{a,b}\mathscr{Z}_4(t) = \beta_1z_2 + \gamma_1z_3 - (\eta + \varrho)z_4. \end{cases} \tag{25}$$

Recall that $\mathscr{R}_0 = \frac{\sigma\nabla((\gamma_1 + \lambda_1 + \eta) + \alpha_1\zeta_1)}{\eta\mathscr{N}(\beta_1 + \zeta_1 + \eta)(\gamma_1 + \lambda_1 + \eta)}$.

Let the bifurcation parameter σ be chosen so that $\mathscr{R}_0 = 1$. Then it follow that $\sigma^* = \frac{\eta\mathscr{N}(\beta_1 + \zeta_1 + \eta)(\gamma_1 + \lambda_1 + \eta)}{\nabla((\gamma_1 + \lambda_1 + \eta) + \alpha_1\zeta_1)}$. The jacobian matrix of the system (25) evaluated at disease-free equilibrium and β_1, is given by

$$J = \begin{pmatrix} -\eta & -\sigma & -\sigma\alpha_2 & -\sigma\alpha_1 \\ 0 & \sigma - (\zeta_1 + \beta_1 + \eta) & \sigma\alpha_2 & \sigma\alpha_1 \\ 0 & \zeta_1 & -(\gamma_1 + \lambda_1 + \eta) & \varrho \\ 0 & \beta_1 & \gamma_1 & -(\varrho + \eta) \end{pmatrix}. \tag{26}$$

This implies a simple zero eigenvalue of the linearized jacobian matrix evaluated at disease-free equilibrium and σ^*, while the remaining eigenvalues have negative real part.

Let the right eigenvector be denoted by $w = (w_1, w_2, w_3, w_4)$. Then the right eigenvector corresponding to the simple zero eigenvalue is obtained, as follow:

$$\begin{cases} -\eta w_1 - \sigma w_2 - \sigma\alpha_2 w_3 - \sigma\alpha_2 w_4 = 0 \\ (1 - p_1))w_2 + \sigma\alpha_2 w_3 + \sigma\alpha_1 w_4 = 0 \\ \zeta w_2 - p_2 w_3 + \varrho w_4 = 0 \\ \beta_1 w_2 + \gamma_1 w_3 - p_3 w_4 = 0. \end{cases} \tag{27}$$

Solving (27) simultaneously, the following result is obtained:

$w_1 = C_3 w_2, \quad w_3 = C_2 w_2, \quad w_4 = C_1 w_2$ where $C_1 = \beta_1 + \frac{\gamma_1 \zeta}{p_2}, \quad C_2 = C_1 + \frac{\zeta}{p_2}, \quad C_3 = \frac{\sigma(1 + a\alpha_2 C_2 + \alpha_2 C_1}{\eta}, \; p_1 = (\zeta_1 + \beta_1 + \eta), \; p_2 = (\gamma_1 + \lambda_1 + \eta)$ and $p_3 = (\rho + \eta)$ In a similar manner, let $v = (v_1, v_2, v_3, v_4)$ be the associated left eigenvector of (26) at *J*, then the left eigenvector is given as:

$$\begin{cases} -\eta v_1 = 0, \\ (\sigma - p_1)v_2 - \zeta v_3 + \beta_1 v_4 = 0, \\ \sigma\alpha_1 v_2 p_2 v_3 + \gamma_1 v_4 = 0, \\ \sigma\alpha_1 v_2 + \varrho v_3 - p_3 v_4 = 0. \end{cases} \tag{28}$$

Solving (28) simultaneously yield the following result

$$v_1 = 0, \quad v_3 = \{\frac{\sigma(\alpha_1 p_3 + \gamma_1 \alpha_2}{p_2 p_3 - \gamma_1 \varrho}\} v_2, \quad v_4 = \{\frac{\sigma(\alpha_2 p_2 + \alpha_1 \varrho)}{p_2 p_3 - \gamma_1 \varrho}\} v_2.$$

Following the approach of[50], we have

$$\bar{a}_1 = v_2 \sum_{k,i,j=1}^{4} w_i w_j \frac{\partial^2 f_1}{\partial x_i \partial x_j} + v_3 \sum_{k,i,j=1}^{4} w_i w_j \frac{\partial^2 f_1}{\partial x_i \partial x_j} + v_4 \sum_{k,i,j=1}^{4} w_i w_j \frac{\partial^2 f_1}{\partial x_i \partial x_j}.$$

$$\bar{b}_1 = v_2 \sum_{k,i=1}^{4} w_i \frac{\partial^2 f_1}{\partial x_i \partial \sigma} + v_3 \sum_{k,i=1}^{4} w_i \frac{\partial^2 f_1}{\partial x_i \partial \sigma} + v_4 \sum_{k,i=1}^{4} w_i \frac{\partial^2 f_1}{\partial x_i \partial \sigma}.$$

$$\frac{\partial^2 f_1}{\partial x_1 \partial x_2} = \frac{\partial^2 f_1}{\partial x_2 \partial x_1} = \frac{\sigma}{\mathcal{N}} \quad \frac{\partial^2 f_1}{\partial x_1 \partial x_3} = \frac{\partial^2 f_1}{\partial x_3 \partial x_1} = \frac{\sigma\alpha_2}{\mathcal{N}} \quad \frac{\partial^2 f_1}{\partial x_1 \partial x_4} = \frac{\partial^2 f_1}{\partial x_4 \partial x_1} = \frac{\sigma\alpha_1}{\mathcal{N}}.$$

$$\frac{\partial^2 f_1}{\partial x_2 \partial \sigma} = \frac{\nabla}{\eta \mathcal{N}}, \quad \frac{\partial^2 f_1}{\partial x_3 \partial \sigma} = \frac{\nabla}{\alpha_2 \mathcal{N}}, \quad \frac{\partial^2 f_1}{\partial x_4 \partial \sigma} = \frac{\nabla}{\alpha_1 \mathcal{N}}.$$

Substituting the above expression into 'a' and 'b' gives

$$\bar{a}_1 = \frac{2v_2 w_1 w_2 \sigma}{\mathcal{N}} + \frac{2v_2 w_1 w_2 \sigma\alpha_2}{\mathcal{N}} + \frac{2v_2 w_1 w_4 \sigma\alpha_1}{\mathcal{N}} \frac{2v_3 w_1 w_2 \sigma}{\mathcal{N}} + \frac{2v_3 w_1 w_2 \sigma\alpha_2}{\mathcal{N}} + \frac{2v_3 w_1 w_4 \sigma\alpha_1}{\mathcal{N}} + \frac{2v_4 w_1 w_2 \sigma}{\mathcal{N}} + \frac{2v_4 w_1 w_2 \sigma\alpha_2}{\mathcal{N}} + \frac{2v_4 w_1 w_4 \sigma\alpha_1}{\mathcal{N}} > 0. \tag{29}$$

$$\bar{b}_1 = \frac{v_2 w_2 \nabla}{\eta \mathcal{N}} + \frac{v_3 w_3 \alpha_2 \nabla}{\eta \mathcal{N}} + \frac{v_4 w_4 \alpha_1 \nabla}{\eta \mathcal{N}} > 0. \tag{30}$$

Both the coefficient of bifurcation present in (29) and (30) are positive so, there exist backward bifurcation in the system.

Existence and uniqueness of solutions

To establish the existence and uniqueness of solutions for the proposed system (5), we employ fixed-point theory, utilizing the Schauder Fixed-Point Theorem for existence and the Banach Contraction Principle for uniqueness[10,62]

Existence results

Assuming the differentiability of the integral, we express the proposed framework as follows. We demonstrate the existence of at least one solution for the considered system (5) using fixed-point theory,

$$\begin{cases} {}^{\mathscr{FFM}}\mathscr{D}_t^{a,b}\mathscr{S}(t) = \nabla - \sigma\left(\frac{\mathscr{I}+\alpha_1\mathscr{T}+\alpha_2\mathscr{A}}{\mathscr{N}}\right)\mathscr{S} - \eta\mathscr{S}, \\ {}^{\mathscr{FFM}}\mathscr{D}_t^{a,b}\mathscr{I}(t) = \sigma\left(\frac{\mathscr{I}+\alpha_1\mathscr{T}+\alpha_2\mathscr{A}}{\mathscr{N}}\right)\mathscr{S} - (\eta+\beta_1+\zeta_1)\mathscr{I}, \\ {}^{\mathscr{FFM}}\mathscr{D}_t^{a,b}\mathscr{A}(t) = \zeta_1\mathscr{I} + \varrho\mathscr{T} - (\gamma_1+\lambda_1+\eta)\mathscr{A}, \\ {}^{\mathscr{FFM}}\mathscr{D}_t^{a,b}\mathscr{T}(t) = \beta_1\mathscr{I} + \gamma_1\mathscr{A} - (\eta+\varrho)\mathscr{T}. \end{cases} \tag{31}$$

We reformulate the model (5) as:

$$\begin{cases} {}^{\mathscr{FFM}}\mathscr{D}_t^{a}\psi(t) = bt^{b-1}\Pi(t,\psi(t)), \\ \psi(0) = \psi_0, \end{cases}$$

where replacing ${}_0^{ABR}\mathscr{D}_0^{a,b}$ with ${}_0^{ABC}\mathscr{D}_0^{a,b}$ and utilizing fractional integrals yields:

$$\psi(t) = \psi(0) + \frac{bt^{b-1}(1-a)}{AB(a)}\Pi(t,\psi(t)) + \frac{ab}{AB(a)\Gamma(a)}\int_0^t \sigma^{b-1}(t-\sigma)^{b-1}\Pi(t,\psi(t))\,d\sigma.$$

Let:

$$\psi(t) = \begin{pmatrix} \mathscr{S}(t) \\ \mathscr{I}(t) \\ \mathscr{A}(t) \\ \mathscr{T}(t) \end{pmatrix}, \quad \psi(0) = \begin{pmatrix} \mathscr{S}(0) \\ \mathscr{I}(0) \\ \mathscr{A}(0) \\ \mathscr{T}(0) \end{pmatrix}, \quad \Pi(t,\psi(t)) = \begin{pmatrix} \boldsymbol{B}_1(t,\mathscr{S},\mathscr{I},\mathscr{A},\mathscr{T}) \\ \boldsymbol{B}_2(t,\mathscr{S},\mathscr{I},\mathscr{A},\mathscr{T}) \\ \boldsymbol{B}_3(t,\mathscr{S},\mathscr{I},\mathscr{A},\mathscr{T}) \\ \boldsymbol{B}_4(t,\mathscr{S},\mathscr{I},\mathscr{A},\mathscr{T}) \end{pmatrix}.$$

Using the Banach space $\mathscr{C} = \mathscr{M}\times\mathscr{M}\times\mathscr{M}\times\mathscr{M}$, where $\mathscr{M} = [0,\tau]$ and norm $\|\psi\| = \max_{t\in[0,\tau]}|\mathscr{S}(t)+\mathscr{I}(t)+\mathscr{A}(t)+\mathscr{T}(t)|$, define the operator $\Pi:\mathscr{C}\to\mathscr{C}$ as:

$$\Pi(\psi)(t) = \psi(0) + \frac{bt^{b-1}(1-a)}{AB(a)}\Omega(t,\psi(t)) + \frac{ab}{AB(a)\Gamma(a)}\int_0^t \sigma^{b-1}(t-\sigma)^{b-1}\Omega(t,\psi(t))\,d\sigma. \tag{32}$$

Assume $\Omega(t,\psi(t))$ satisfies the following:

- Growth bound: $\exists\ \ Q_\Omega, \mathscr{W}_\Omega > 0$ such that

$$|\Omega(t,\psi(t))| \le Q_\Omega|\psi(t)| + \mathscr{W}_\Omega. \tag{33}$$

- Lipschitz continuity: $\exists\ \ \mathscr{P}_\Omega > 0$ such that

$$|\Omega(t,\psi(t)) - \Omega(t,\overline{\psi}(t))| \le \mathscr{P}_\Omega|\psi(t)-\overline{\psi}(t)|. \tag{34}$$

Theorem 5 *Suppose the condition (33) holds. Let $\Omega:[0,\tau]\times\mathscr{C}\to\mathscr{R}$ be a continuous function. Therefore, the proposed model possesses at least one solution.*

Proof Initially, we must demonstrate that the operator Π defined by (32) exhibits complete continuity. As Ω is continuous, it follows that Π is also continuous.

Let $\mathscr{M} = \{\psi\in\mathscr{C} : \|\psi\| \le \mathscr{R}, \mathscr{R} > 0\}$. Now for any $\psi\in\mathscr{C}$, we have

$$\begin{aligned} |\Pi(\psi)| =& max_{t\in[0,\tau]}\left|\psi(0) + \frac{bt^{b-1}(1-a)}{AB(a)}\Omega(t,\psi(t)) + \frac{ab}{AB(a)\Gamma(a)}\int_0^t \sigma^{b-1}\,(t-\sigma)^{b-1}\,\Omega(t,\psi(t))d\sigma\right| \\ \le& \psi(0) + \frac{bt^{b-1}(1-a)}{AB(a)}(Q_\Omega\,\|\psi\| + \mathscr{W}_\Omega) + max_{t\in[0,\tau]}\frac{ab}{AB(a)\Gamma(a)}\int_0^t \sigma^{b-1}\,(t-\sigma)^{b-1}\,|\Omega(\sigma,\psi(\sigma))|\,d\sigma \\ \le& \psi(0) + \frac{bt^{b-1}(1-a)}{AB(a)}(Q_\Omega\,\|\psi\| + \mathscr{W}_\Omega) + \frac{ab}{AB(a)\Gamma(a)}(Q_\Omega\,\|\psi\| + \mathscr{W}_\Omega)t^{b-1}\mathscr{M}(a,b) \\ \le& \mathscr{R}. \end{aligned}$$

Therefore, the operator Π is uniformly bounded, with $\mathscr{M}(a,b)$ denoting the beta function.

For equi-continuity of Π let us take $t_1 < t_2 \le \tau$ then consider,

$$
\begin{aligned}
|\Pi(\psi)(t_2)-\Pi(\psi)(t_1)| =& \left|\left(\frac{bt_2^{b-1}(1-a)}{AB(a)}\Omega(t_2,\psi(t_2))+\frac{ab}{AB(a)\Gamma(a)}\int_0^{t_2}\sigma^{b-1}\left(t_2-\sigma\right)^{b-1}\Omega(\sigma,\psi(\sigma))d\sigma\right)\right. \\
&\left.-\left(\frac{bt_1^{b-1}(1-a)}{AB(a)}\Omega(t_1,\psi(t_1))+\frac{ab}{AB(a)\Gamma(a)}\int_0^{t_1}\sigma^{b-1}\left(t_1-\sigma\right)^{b-1}\Omega(\sigma,\psi(\sigma))d\sigma\right)\right| \\
\leq& \frac{bt_2^{b-1}(1-a)}{AB(a)}(Q_\Omega|\psi(t)|+\mathscr{W}_\Omega)+\frac{ab}{AB(a)\Gamma(a)}(Q_\Omega|\psi(t)|+\mathscr{W}_\Omega)t_2^{a+b-1}\mathscr{M}(a,b) \\
&-\frac{bt_1^{b-1}(1-a)}{AB(a)}(Q_\Omega|\psi(t)|+\mathscr{W}_\Omega)-\frac{ab}{AB(a)\Gamma(a)}(Q_\Omega|\psi(t)|+\mathscr{W}_\Omega)t_1^{a+b-1}\mathscr{M}(a,b),
\end{aligned}
$$

when $t_1 \to t_2$then $|\Pi(\psi)(t_2)-\Pi(\psi)(t_1)| \to 0$. Consequently, we can say that
$\|\Pi(\psi)(t_2)-\Pi(\psi)(t_1)\| \to 0$, as $t_1 \to t_2$.

Consequently, Π is equi-continuous. Thus, by the Arzelá-Ascoli theorem, it is completely continuous. Therefore, according to fixed-point Schauder's theorem, the suggested framework possesses at least a singular solution. □

Theorem 6 *Presume that* (34) *applies. If* $\varrho < 1$, *where*

$$
\varrho = \left(\frac{bt_2^{b-1}(1-a)}{AB(a)}+\frac{ab}{AB(a)\Gamma(a)}t^{a+b-1}\mathscr{M}(a,b)\right)\mathscr{P}_\Omega.
$$

Hence, the model question has a unique solution.

Proof For any $\psi, \overline{\psi} \in \mathscr{C}$, we obtain

$$
\begin{aligned}
\left|\Pi(\psi)-\Pi(\overline{\psi})\right| =& max_{t\in[0,\tau]}\mid \frac{bt^{b-1}(1-a)}{AB(a)}(\Omega(t,\psi(t))-\Omega(t,\overline{\psi}(t))) \\
&+\frac{ab}{AB(a)\Gamma(a)}\int_0^t \sigma^{b-1}\left(t-\sigma\right)^{b-1}d\sigma(\Omega(\sigma,\psi(\sigma))-\Omega(\sigma,\overline{\psi}(\sigma)))\mid \\
\leq& \left[\frac{bt^{b-1}(1-a)}{AB(a)}+\frac{ab}{AB(a)\Gamma(a)}t^{a+b-1}\mathscr{M}(a,b)\right]\left\|\psi-\overline{\psi}\right\| \\
\leq& \varrho\left\|\psi-\overline{\psi}\right\|.
\end{aligned}
$$

Thus, Π functions as a contraction. Therefore, by the Banach contraction theorem, the proposed model has a unique solution. □

Numerical analysis

In this section, we develop a computational scheme to efficiently solve the system while accurately capturing the effects of fractional derivatives. Traditional numerical methods often struggle with fractional-order systems due to their nonlocal properties, requiring careful handling of past states[38,53]. To overcome these limitations, we combine Atangana-Baleanu fractional operators (under the Caputo definition) with the Adams-Bashforth numerical scheme[63,64]. This hybrid strategy leverages the multi-step nature of Adams-Bashforth-which reuses prior computational results to minimize processing demands-while the fractional operators account for memory effects and non-local interactions inherent to HIV/AIDS dynamics. By refining past state estimates through interpolation, the method sharpens accuracy without substantially increasing computational costs, a critical advantage for modeling long-term disease progression. The approach also inherently suppresses numerical oscillations common in fractional-order systems, ensuring stable simulations even when capturing abrupt shifts in transmission rates or treatment delays.

The computational demands of our method arise from fractional derivatives' reliance on past states, which necessitate storing and processing historical data[65,66]. While this approach imposes a higher computational burden compared to classical models, the Adam-Bashforth method optimize efficiency by strategically reusing previously computed results. Although the method is scalable for epidemiological applications, its performance can be further improved through adaptive step-size control, parallel processing, or the implementation of sparse memory techniques[67]. For instance, fast convolution algorithms could expedite simulations when applied to region-specific datasets. Parameter values in this study align with established theoretical frameworks for HIV/AIDS modeling, prioritizing generality over region-specific calibration. This approach isolates core dynamics-such as stability thresholds and sensitivity to memory effects-while avoiding biases from empirical data variability. By systematically testing fractional orders, we dissect how historical dependencies (e.g., delayed treatment access or lingering immunity) influence outbreak trajectories and control efficacy. Building on this foundation, we adapt the governing system (5) using the Adams-Bashforth scheme, embedding Atangana-Baleanu integrals to couple memory effects with iterative computation. The reformulated system becomes:

$$\begin{cases} \mathscr{S}(t) = \mathscr{S}(0) + \frac{bt^{b-1}(1-a)}{AB(a)}\boldsymbol{Z}_1(t,\mathscr{S},\mathscr{I},\mathscr{A},\mathscr{T}) \\ \quad + \frac{ab}{AB(a)\Gamma(a)}\int_0^t \sigma^{b-1}(t-\sigma)\boldsymbol{Z}_1(\sigma,\mathscr{S},\mathscr{I},\mathscr{A},\mathscr{T})d\sigma, \\ \mathscr{I}(t) = \mathscr{I}(0) + \frac{bt^{b-1}(1-a)}{AB(a)}\boldsymbol{Z}_2(t,\mathscr{S},\mathscr{I},\mathscr{A},\mathscr{T}) \\ \quad + \frac{ab}{AB(a)\Gamma(a)}\int_0^t \sigma^{b-1}(t-\sigma)\boldsymbol{Z}_2(\sigma,\mathscr{S},\mathscr{I},\mathscr{A},\mathscr{T})d\sigma, \\ \mathscr{A}(t) = \mathscr{A}(0) + \frac{bt^{b-1}(1-a)}{AB(a)}\boldsymbol{Z}_3(t,\mathscr{S},\mathscr{I},\mathscr{A},\mathscr{T}) \\ \quad + \frac{ab}{AB(a)\Gamma(a)}\int_0^t \sigma^{b-1}(t-\sigma)\boldsymbol{Z}_3(\sigma,\mathscr{S},\mathscr{I},\mathscr{A},\mathscr{T})d\sigma, \\ \mathscr{T}(t) = \mathscr{T}(0) + \frac{bt^{b-1}(1-a)}{AB(a)}\boldsymbol{Z}_4(t,\mathscr{S},\mathscr{I},\mathscr{A},\mathscr{T}) \\ \quad + \frac{ab}{AB(a)\Gamma(a)}\int_0^t \sigma^{b-1}(t-\sigma)\boldsymbol{Z}_4(\sigma,\mathscr{S},\mathscr{I},\mathscr{A},\mathscr{T})d\sigma. \end{cases} \tag{35}$$

The first step to build a numerical scheme at time step $t = t_{n+1}$. involves transforming governing equations to show state variable changes between time intervals. Turning continuous-time dynamics into suitable format for iterative solvers requires implementing discrete-time discrete solutions.

$$\begin{cases} \mathscr{S}^{n+1} = \mathscr{S}^0 + \frac{bt^{b-1}(1-a)}{AB(a)}\boldsymbol{Z}_1(t_n,\mathscr{S}^n,\mathscr{I}^n,\mathscr{A}^n,\mathscr{T}^n) \\ \quad + \frac{ab}{AB(a)\Gamma(a)}\int_0^t \sigma^{b-1}(t-\sigma)^{b-1}\boldsymbol{Z}_1(\sigma,\mathscr{S},\mathscr{I},\mathscr{A},\mathscr{T})d\sigma, \\ \mathscr{I}^{n+1} = \mathscr{I}^0 + \frac{bt^{b-1}(1-a)}{AB(a)}\boldsymbol{Z}_2(t_n,\mathscr{S}^n,\mathscr{I}^n,\mathscr{A}^n,\mathscr{T}^n) \\ \quad + \frac{ab}{AB(a)\Gamma(a)}\int_0^t \sigma^{b-1}(t-\sigma)^{b-1}\boldsymbol{Z}_2(\sigma,\mathscr{S},\mathscr{I},\mathscr{A},\mathscr{T})d\sigma, \\ \mathscr{A}^{n+1} = \mathscr{A}^0 + \frac{bt^{b-1}(1-a)}{AB(a)}\boldsymbol{Z}_3(t_n,\mathscr{S}^n,\mathscr{I}^n,\mathscr{A}^n,\mathscr{T}^n) \\ \quad + \frac{ab}{AB(a)\Gamma(a)}\int_0^t \sigma^{b-1}(t-\sigma)^{b-1}\boldsymbol{Z}_3(\sigma,\mathscr{S},\mathscr{I},\mathscr{A},\mathscr{T})d\sigma, \\ \mathscr{T}^{n+1} = \mathscr{T}^0 + \frac{bt^{b-1}(1-a)}{AB(a)}\boldsymbol{Z}_4(t_n,\mathscr{S}^n,\mathscr{I}^n,\mathscr{A}^n,\mathscr{T}^n) \\ \quad + \frac{ab}{AB(a)\Gamma(a)}\int_0^t \sigma^{b-1}(t-\sigma)^{b-1}\boldsymbol{Z}_4(\sigma,\mathscr{S},\mathscr{I},\mathscr{A},\mathscr{T})d\sigma. \end{cases} \tag{36}$$

The integral terms of Equation (36) require piecewise Lagrangian interpolation across each subinterval $[t_m, t_{m+1}]$. The computational method uses this precision-effective approach to yield the following numerical iteration scheme:

$$\begin{cases} \mathscr{S}^{n+1} = \mathscr{S}^0 + \frac{bt_n^{b-1}(1-a)}{AB(a)}\boldsymbol{Z}_1(t_n,\mathscr{S}^n,\mathscr{I}^n,\mathscr{A}^n,\mathscr{T}^n) \\ \quad + \frac{ab}{AB(a)\Gamma(a)}\sum_{m=0}^{n} A_m(\sigma), \\ \mathscr{I}^{n+1} = \mathscr{I}^0 + \frac{bt_n^{b-1}(1-a)}{AB(a)}\boldsymbol{Z}_2(t_n,\mathscr{S}^n,\mathscr{I}^n,\mathscr{A}^n,\mathscr{T}^n) \\ \quad + \frac{ab}{AB(a)\Gamma(a)}\sum_{m=0}^{n} B_m(\sigma), \\ \mathscr{A}^{n+1} = \mathscr{A}^0 + \frac{bt_n^{b-1}(1-a)}{AB(a)}\boldsymbol{Z}_3(t_n,\mathscr{S}^n,\mathscr{I}^n,\mathscr{A}^n,\mathscr{T}^n) \\ \quad + \frac{ab}{AB(a)\Gamma(a)}\sum_{m=0}^{n} C_m(\sigma), \\ \mathscr{T}^{n+1} = \mathscr{T}^0 + \frac{bt_n^{b-1}(1-a)}{AB(a)}\boldsymbol{Z}_4(t_n,\mathscr{S}^n,\mathscr{I}^n,\mathscr{A}^n,\mathscr{T}^n) \\ \quad + \frac{ab}{AB(a)\Gamma(a)}\sum_{m=0}^{n} D_m(\sigma). \end{cases} \tag{37}$$

The numerical outputs obtained from a fractional differential system are contained in Equation (5). The piecewise interpolation technique improves accuracy by involving local integrations of terms which preserves the model dynamics.

$$\begin{cases} A_m(\sigma) = \frac{\sigma-t_{m-1}}{t_m-t_{m-1}}t_m^b\boldsymbol{Z}_1(t,\mathscr{S},\mathscr{I},\mathscr{A},\mathscr{T}) - \frac{\sigma-t_m}{t_m-t_{m-1}}t_{m-1}^{b-1}\boldsymbol{Z}_1(t_n,\mathscr{S}^{m-1},\mathscr{I}^{m-1},\mathscr{A}^{m-1},\mathscr{T}^{m-1}), \\ B_m(\sigma) = \frac{\sigma-t_{m-1}}{t_m-t_{m-1}}t_m^b\boldsymbol{Z}_2(t,\mathscr{S},\mathscr{I},\mathscr{A},\mathscr{T}) - \frac{\sigma-t_m}{t_m-t_{m-1}}t_{m-1}^{b-1}\boldsymbol{Z}_2(t_n,\mathscr{S}^{m-1},\mathscr{I}^{m-1},\mathscr{A}^{m-1},\mathscr{T}^{m-1}), \\ C_m(\sigma) = \frac{\sigma-t_{m-1}}{t_m-t_{m-1}}t_m^b\boldsymbol{Z}_3(t,\mathscr{S},\mathscr{I},\mathscr{A},\mathscr{T}) - \frac{\sigma-t_m}{t_m-t_{m-1}}t_{m-1}^{b-1}\boldsymbol{Z}_3(t_n,\mathscr{S}^{m-1},\mathscr{I}^{m-1},\mathscr{A}^{m-1},\mathscr{T}^{m-1}), \\ D_m(\sigma) = \frac{\sigma-t_{m-1}}{t_m-t_{m-1}}t_m^b\boldsymbol{Z}_4(t,\mathscr{S},\mathscr{I},\mathscr{A},\mathscr{T}) - \frac{\sigma-t_m}{t_m-t_{m-1}}t_{m-1}^{b-1}\boldsymbol{Z}_4(t_n,\mathscr{S}^{m-1},\mathscr{I}^{m-1},\mathscr{A}^{m-1},\mathscr{T}^{m-1}). \end{cases}$$

Utilizing Lagrangian polynomial piecewise interpolation, we obtain

$$
\begin{cases}
\mathscr{S}^{n+1} = \mathscr{S}^{0} + \frac{bt_n^{b-1}(1-a)}{AB(a)}\boldsymbol{Z}_1(t_n,\mathscr{S}^n,\mathscr{I}^n,\mathscr{A}^n,\mathscr{T}^n) + \frac{ab}{AB(a)\Gamma(a)} \\
\sum_{m=0}^{n}\left[\begin{array}{l} t_n^{b-1}\boldsymbol{Z}_1(t_n,\mathscr{S}^n,\mathscr{I}^n,\mathscr{A}^n,\mathscr{T}^n)((n+1-m)^a(n-m+2+a)-(n-m)^a(2+2a+n-m)) \\ -t_{n-1}^{b-1}\boldsymbol{Z}_1(t_{n-1},\mathscr{S}^{n-1},\mathscr{I}^{n-1},\mathscr{A}^{n-1},\mathscr{T}^{n-1})((1+n-m)^{a+1}-(n-m)^a(1+a+n-m)) \end{array}\right], \\
\mathscr{I}^{n+1} = \mathscr{I}^{0} + \frac{bt_n^{b-1}(1-a)}{AB(a)}\boldsymbol{Z}_2(t_n,\mathscr{S}^n,\mathscr{I}^n,\mathscr{A}^n,\mathscr{T}^n) + \frac{ab}{AB(a)\Gamma(a)} \\
\sum_{m=0}^{n}\left[\begin{array}{l} t_n^{b-1}\boldsymbol{Z}_2(t_n,\mathscr{S}^n,\mathscr{I}^n,\mathscr{A}^n,\mathscr{T}^n)((n+1-m)^a(n-m+2+a)-(n-m)^a(2+2a+n-m)) \\ -t_{n-1}^{b-1}\boldsymbol{Z}_2(t_{n-1},\mathscr{S}^{n-1},\mathscr{I}^{n-1},\mathscr{A}^{n-1},\mathscr{T}^{n-1})((1+n-m)^{a+1}-(n-m)^a(1+a+n-m)) \end{array}\right], \\
\mathscr{A}^{n+1} = \mathscr{A}^{0} + \frac{bt_n^{b-1}(1-a)}{AB(a)}\boldsymbol{2}_3(t_n,\mathscr{S}^n,\mathscr{I}^n,\mathscr{A}^n,\mathscr{T}^n) + \frac{ab}{AB(a)\Gamma(a)} \\
\sum_{m=0}^{n}\left[\begin{array}{l} t_n^{b-1}\boldsymbol{Z}_3(t_n,\mathscr{S}^n,\mathscr{I}^n,\mathscr{A}^n,\mathscr{T}^n)((n+1-m)^a(n-m+2+a)-(n-m)^a(2+2a+n-m)) \\ -t_{n-1}^{b-1}\boldsymbol{Z}_3(t_{n-1},\mathscr{S}^{n-1},\mathscr{I}^{n-1},\mathscr{A}^{n-1},\mathscr{T}^{n-1})((1+n-m)^{a+1}-(n-m)^a(1+a+n-m)) \end{array}\right], \\
\mathscr{T}^{n+1} = \mathscr{T}^{0} + \frac{bt_n^{b-1}(1-a)}{AB(a)}\boldsymbol{Z}_4(t_n,\mathscr{S}^n,\mathscr{I}^n,\mathscr{A}^n,\mathscr{T}^n) + \frac{ab}{AB(a)\Gamma(a)} \\
\sum_{m=0}^{n}\left[\begin{array}{l} t_n^{b-1}\boldsymbol{Z}_4(t_n,\mathscr{S}^n,\mathscr{I}^n,\mathscr{A}^n,\mathscr{T}^n)((n+1-m)^a(n-m+2+a)-(n-m)^a(2+2a+n-m)) \\ -t_{n-1}^{b-1}\boldsymbol{Z}_4(t_{n-1},\mathscr{S}^{n-1},\mathscr{I}^{n-1},\mathscr{A}^{n-1},\mathscr{T}^{n-1})((1+n-m)^{a+1}-(n-m)^a(1+a+n-m)) \end{array}\right].
\end{cases} \tag{38}
$$

Equation (38) depicts the overall numerical outcomes of the analyzed system.

The initial data, we assumed as $\mathscr{S}(0) = 0.10, \quad \mathscr{I}(0) = 0.50, \quad \mathscr{A}(0) = 0.10, \quad \mathscr{T}(0) = 0.300.$ in millions and the following parameters values given in Table 2 were assumed on the basis of this data.

Computational experiments and results

This section presents computational experiments evaluating the effectiveness of the proposed fractal-fractional model in capturing HIV/AIDS transmission and treatment dynamics. The fractional-order framework enhances epidemiological modeling by accurately representing memory effects and long-term dependencies in disease progression. Compared to previous studies on the interplay of HIV/AIDS with co-infections and fractional-order epidemic models[65,67], our approach provides a more refined analysis of disease interactions and treatment impact. Numerical simulations were conducted using theoretically estimated parameter values (listed in **Table 2**). To investigate the influence of different fractional orders, we perform simulations for various values of r, examining their impact on system stability and convergence behavior.

Figure 4(a)–4(d) illustrate the evolution of susceptible individuals, infected individuals, individuals progressing to AIDS, and treated individuals for fractional orders $r = (0.25, 0.25), (0.35, 0.30), (0.45, 0.35)$, and $(0.55, 0.40)$. In all cases, the system trajectories consistently converge to the endemic equilibrium, highlighting the stability of the model. However, variations in the fractional order influence the rate of convergence, with lower values of r leading to faster stabilization, whereas higher values introduce more oscillatory behavior. Further simulations for higher fractional orders ($r = (0.65, 0.85)$, $(0.75, 0.90)$, $(0.85, 0.95)$, and $(0.95, 1.0)$), presented in Fig. 5(a)–5(d), reveal an increasing tendency toward complex, oscillatory patterns in the disease dynamics. The impact of fractional order r on the progression of treated individuals is further analyzed in Fig. 6(a)–6(d). The results confirm that while the system remains stable across all tested values, lower fractional orders favor faster disease suppression, whereas higher orders reflect more prolonged treatment response times. This is due to the stronger historical influence retained by higher-order derivatives, mirroring real-world scenarios where treatment efficacy is affected by factors such as adherence and immune response variability. Figs. 7(a)–7(d) and 8(a), 8(b) offer further insights into the complex dynamics of disease transmission, treatment efficacy, and the influence of memory effects.

The system generates chaotic oscillations instead of smooth trajectories under specific parameter values which are shown in Fig. 8(a)-8(b). The stable equilibrium state positions shift instantly because of tiny fractional order r alterations near bifurcation points. The analysis of delayed control measures and rapid disease outbreaks related to immunological deterioration can be simulated through these identified tendencies. The disease dynamics become linked to fractional order r through the distribution of S for susceptible and I for infected between x-axis and y-axis. When r value reduces in forecasting scenarios the prediction instability rises while previous disease outbreaks and unstable medical service distribution intensify this condition. The transmission system functions smoothly with growing values of r that support advanced implementation of ART as well as sustained preventive measures. The time-dependent quantities of viral load and treatment coverage serve as vertical

Parameter	Value 1	Value 2
∇	1.68	1.80
α_1	0.01234	1.05
α_2	0.8921	1.15
η	0.00826	0.03
β_1	0.005089	1.10
λ_1	0.0803	0.01
ϱ	0.09876	0.11
ζ_1	0.0803	0.01
σ	0.0964	0.12
γ_1	0.0951	0.01

Table 2. Model parameters with their numerical values.

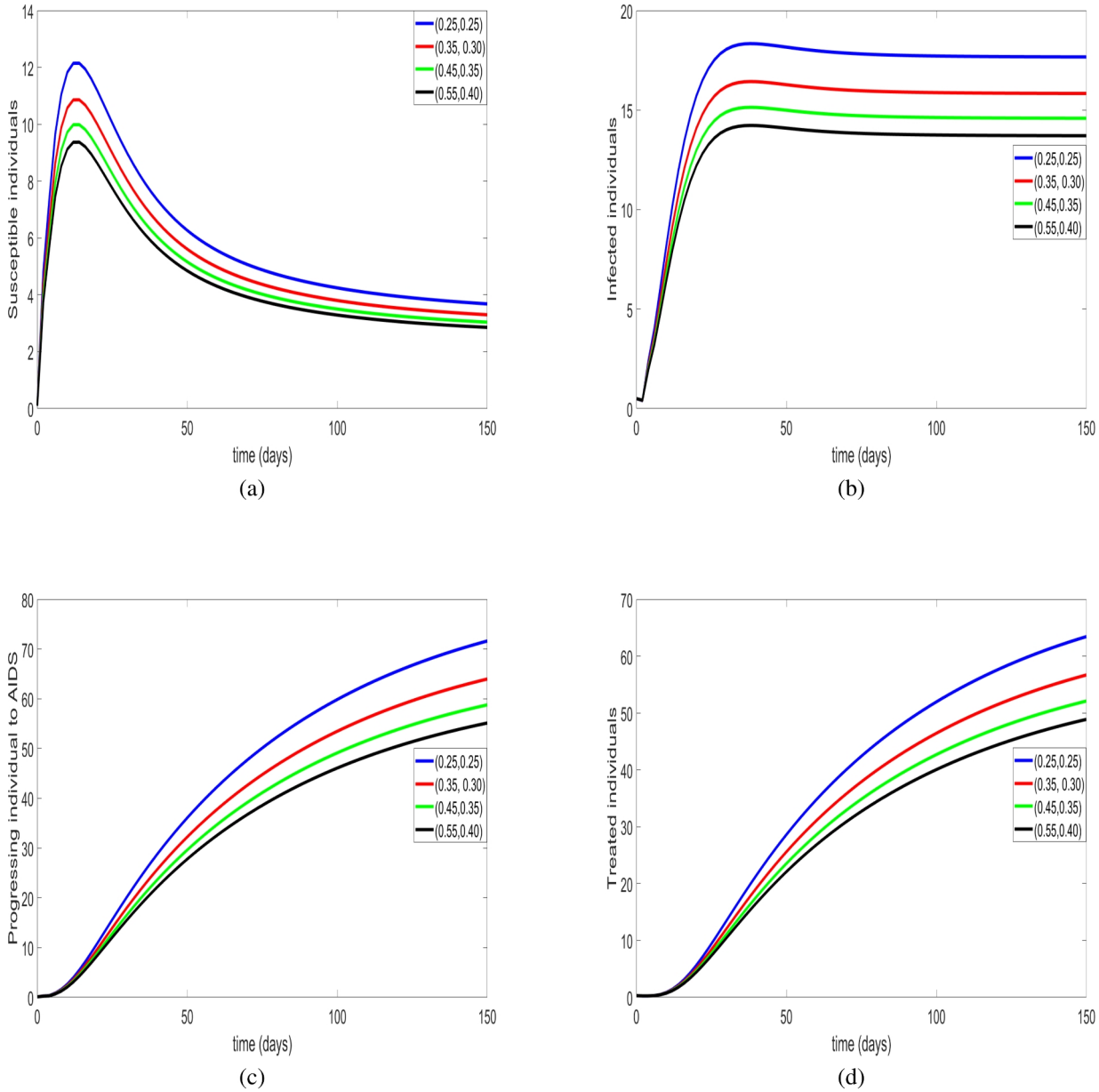

Fig. 4. Dynamics of the system for fractional orders $r = (0.25, 0.25), (0.35, 0.30), (0.45, 0.35)$, and (0.55, 0.40) depicted. These plots present the evolution of susceptible, infected, treated, and AIDS-stage populations using different fractional orders. Modifying orders in the model framework results in transformations of disease spread patterns, ranging from brief control periods to extended endemic conditions. These simulated effects show both healthcare disparities in real forms and the timing methods used in practical intervention procedures.

values (z-axis coordinates) throughout Figs. 9(a)-10(b). Healthcare implementations of enhanced r values develop standardized forecasting methods which operate like well-designed surveillance systems but reduce the sensitivity of initial settings. The incorporation of fractional calculus allows theoretical models and real-life complex systems to connect with expert testimony in research structures. The r variable enables such methods to modify forecasts based on previous effect patterns in systems with changing variables. Epidemiological analysis in modern times depends on this model because it delivers essential data needed for healthcare sector resource allocation and planning assessment.

The system develops chaotic behavior when fractional order parameters exceed specific thresholds and keep treatment parameters static. As a result equilibrium is disrupted. The model consists of several factors which demonstrate HIV/AIDS complexities by showcasing drug resistance along with different immune system responses that lead to possible new infections. Laboratory variabilities and intervention delays negatively affect model accuracy by making disease progression abruptly quick during such periods. Fractal-fractional differential

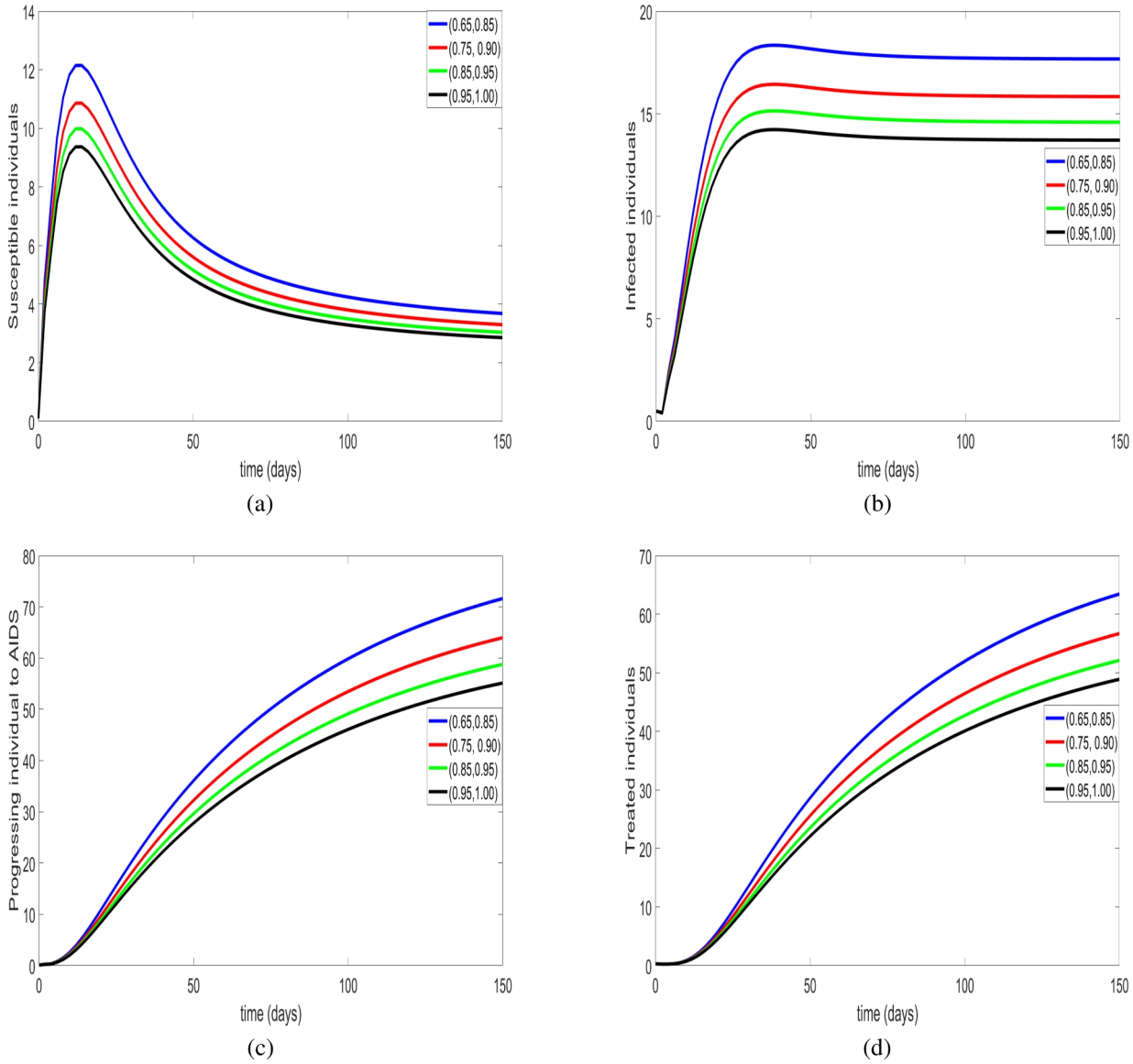

Fig. 5. System dynamics for fractional orders $r = (0.5, 0.75), (0.6, 0.80), (0.7, 0.85)$, and $(0.8, 0.90)$, showcasing the impact of varying fractional-order parameters. This information demonstrates how fractional orders affect the distribution between susceptible individuals and infected patients, in addition to disease progression and treatment detection for AIDS. The provided data allows the fractional-order modeling system to reproduce multiple transmission occurrences.

modeling allows the FFOD to deliver superior accuracy compared to traditional integer-order models because it considers memoryless transitions in numerical descriptions.

Data analysis through this metric proves better than conventional means to predict disease progression because it provides improved stability and predictive ability especially for illnesses with extended latency following treatment. Rather than relying on real-world empirical validation, these numerical results reinforce the theoretical framework of the proposed model.

Chaotic trajectories illustrating the relationship between the **susceptible population** (S) and **infected population** (I) under different fractional-order dynamics. Fig. 8 (a) shows more pronounced chaotic behavior, while Fig. 8 (b) demonstrates smoother, more stable trajectories as the fractional order increases.

The x-axis represents S (susceptible individuals), the y-axis denotes I (infected individuals), and the z-axis corresponds to T (Treated individuals). Figure 9 (a) presents system behavior for lower fractional orders and showing more variation. Also, Fig. 9 (b) illustrates higher fractional orders, exhibiting a more stable and structured progression.

The fractional-order derivatives successfully encapsulate memory effects, providing a more nuanced representation of HIV/AIDS transmission and intervention strategies. Graphical analysis confirm that fractional-order models, particularly for smaller values of r, mitigate instability and chaotic fluctuations, making them a promising alternative to conventional epidemiological models. These determination underline the requisite

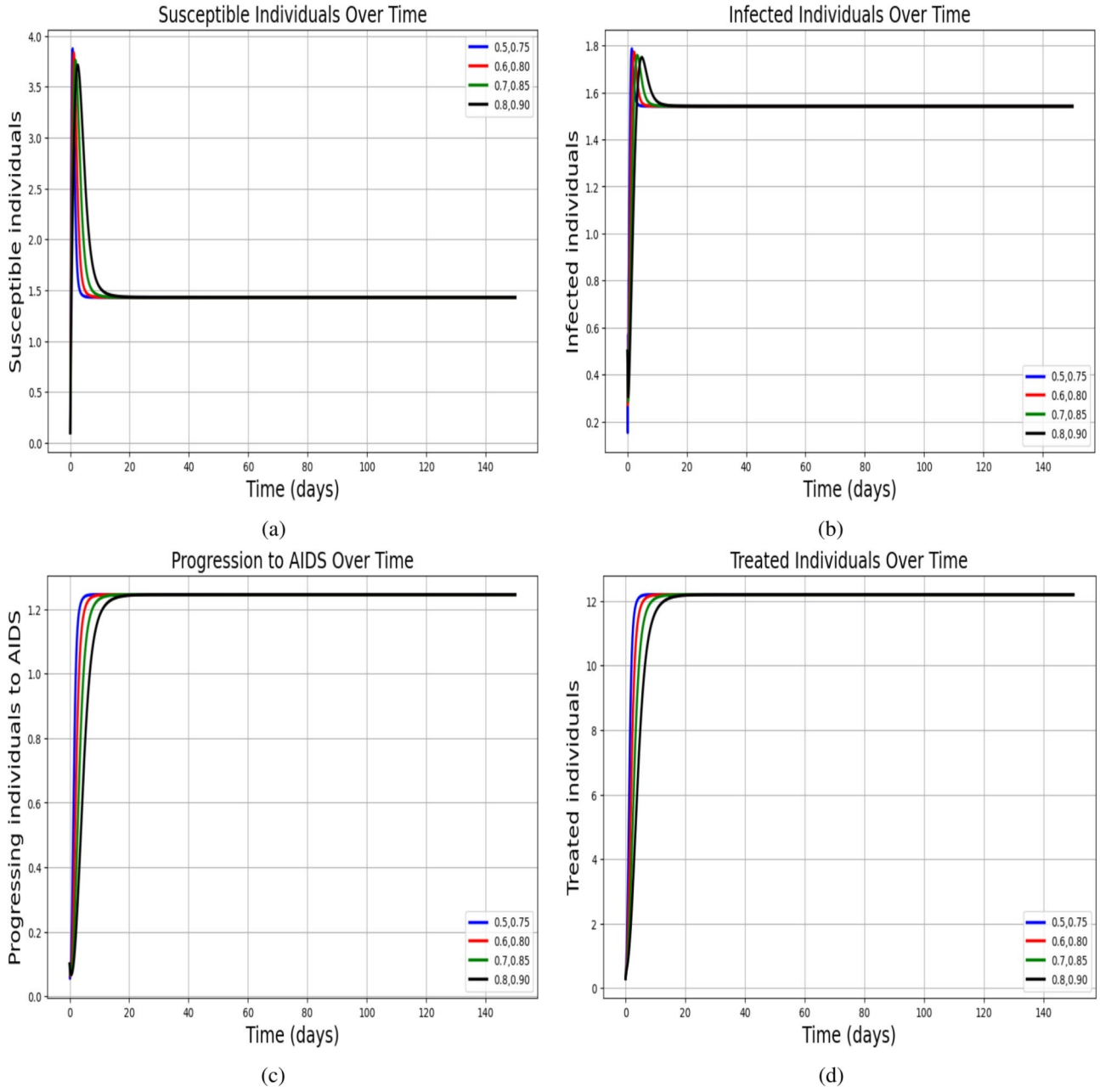

Fig. 6. System dynamics for fractional orders $r = (0.65, 0.85), (0.75, 0.90), (0.85, 0.95)$, and (0.95, 1.0), illustrating the behavior under varying fractional-order parameters. Several graphs display the temporal changes of population segments, which comprise susceptible individuals alongside infected individuals and people who progress to AIDS while in the treatment phase. These graphs use multiple fractional-order values. The authors present how this system responds during various transmission scenarios inside fractional-order structures.

of fractional calculus in epidemiological modeling, present deeper insights into the fundamental mechanisms governing disease progression, control measures, and potential intervention outcomes. Future extensions of this work could explore real-world data fitting, stochastic extensions, or multi-scale modeling tactic to further rectify the applicability of fractional-order epidemiological models. Further, some details about the dynamical behaviour has shown in Fig. 10 (a) and Fig. 10 (b) respectively.

The x-axis represents S (susceptible population), the y-axis represents$I$ (infected population), and the z-axis represents the fractional-order effects. Figure 10 (a) demonstrates higher variability, whereas Fig. 10 (b) displays a more structured and stable pattern.

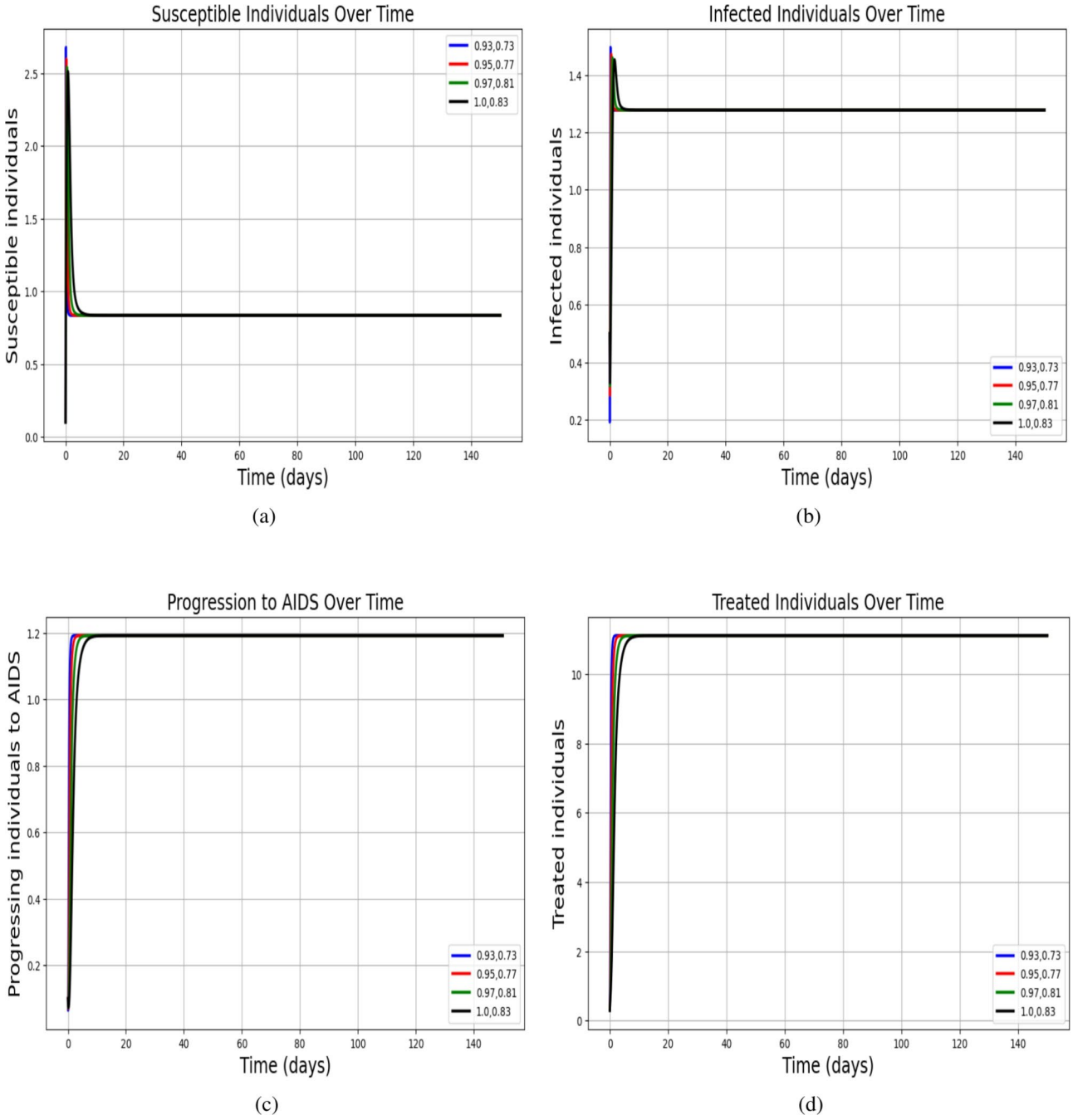

Fig. 7. Dynamics of the system for fractional orders $r = (0.93, 0.73), (0.95, 0.77), (0.97, 0.81)$, and (1.0, 0.83), highlighting the influence of varying fractional-order parameters on system behavior. These figures illustrate the dynamics of susceptible individuals, infected individuals, disease progression to AIDS, and treated individuals under varying fractional orders. They highlight the system's behavior across different transmission scenarios within a fractional-order modeling framework, providing insights into the impact of fractional dynamics on disease spread and treatment outcomes.

Discussion

The proposed fractal-fractional model introduces an innovative framework for characterizing the intricate dynamics disease transmission[4–6]. By incorporating fractal derivatives[48,68] and fractional order calculus, the model provides a more versatile and comprehensive representation of memory effects and hereditary properties, which are frequently neglected in traditional integer-order frameworks[37,69]. Fractal component encodes the irregular and self-similar character of real world interactions, while the fractional-order formulation captures long-range dependencies and non-local effect in disease spread. This combined proposed model provides a more complete perspective on epidemiological processes than traditional compartmental frameworks[30,31].

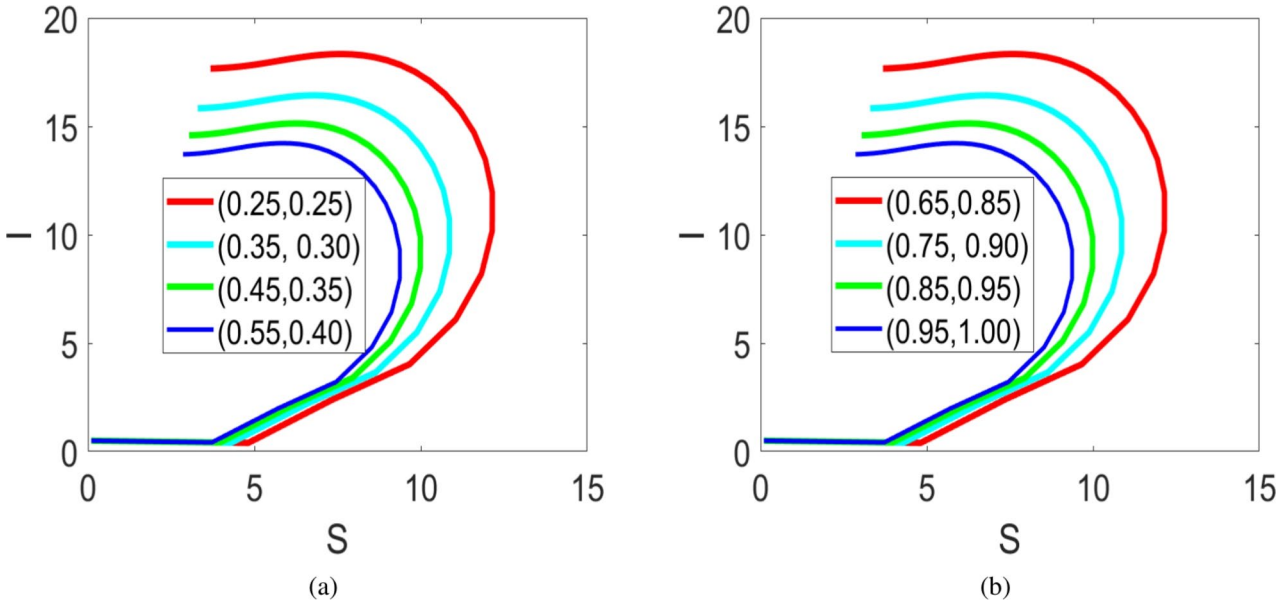

Fig. 8. Chaotic curves for fractional orders r = (0.25, 0.25), (0.35, 0.30), (0.45, 0.35), (0.55, 0.40), (0.65, 0.85), (0.75, 0.90), (0.85, 0.95), and (0.95, 1.0), illustrating the complex dynamics of the system under varying fractional-order parameters.

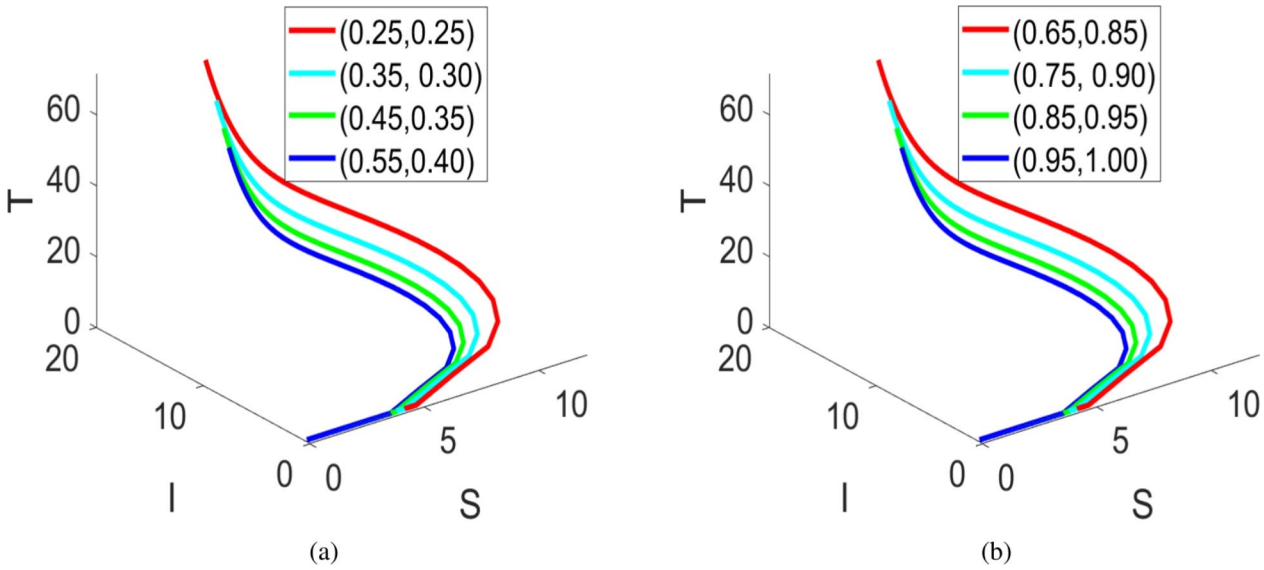

Fig. 9. Three-dimensional trajectories of our model for HIV dynamics, illustrating the evolution of the system for different fractional orders.

Compared to standard frameworks, the advantages of the fractal-fractional framework are evident. Traditional integer-order frameworks, e.g., the standard Susceptible-infected-Recovered (SIR) framework[70], rely on local and Markovian dynamics that generally are not able to capture the persistence and complexity of disease transmission[71]. While fractional-order models improve upon this by introducing memory-dependent dynamics, they do not explicitly consider the fractal structure of human interactions[65,66]. In contrast, the fractal-fractional model unifies these aspects, offering a richer and more realistic mathematical representation of epidemic spread. Furthermore, numerical simulations demonstrate that the model exhibits superior flexibility in fitting empirical data and capturing diverse epidemic scenarios[32,46,67].

While our model offers valuable insights, several limitations warrant discussion. The assumption of homogeneous mixing-where all individuals interact uniformly-ignores real-world complexities like clustered social networks, geographic disparities in healthcare access, and demographic variability[72]. This simplification may underestimate transmission hotspots in urban centers or marginalized communities. Future studies could

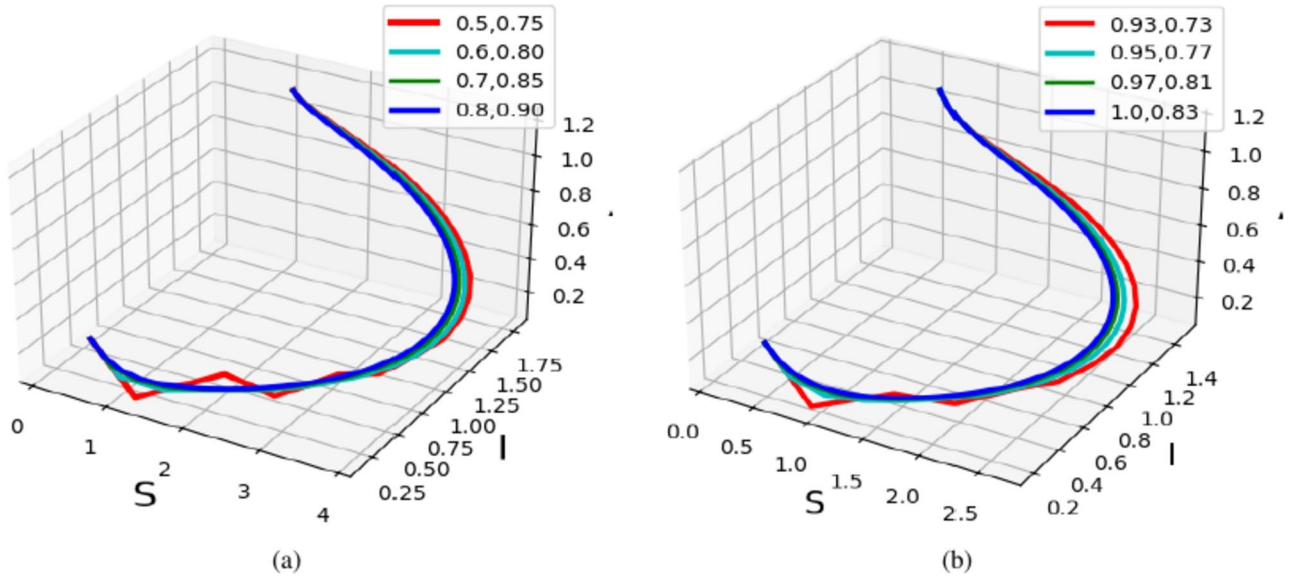

Fig. 10. Three-dimensional system dynamics for fractional orders r = (0.5, 0.75), (0.6, 0.80), (0.7, 0.85), (0.8, 0.90), r = (0.93, 0.73), (0.95, 0.77), (0.97, 0.81), and (1.0, 0.83).

introduce spatially explicit compartments, stochastic terms to model random super spreader events, or age-stratified contact patterns to better align with empirical data[73]. Further refining the framework through hof bifurcation analysis could uncover tipping points in treatment efficacy or immunity thresholds, while integrating optimal control theory might identify cost-effective intervention schedules. Empirical validation using regional HIV incidence data, paired with Bayesian parameter calibration, would strengthen predictive reliability for localized policymaking[74]. Despite these gaps, the study demonstrates how fractal-fractional models bridge traditional epidemiological frameworks and the nonlinear, memory-driven reality of disease spread-a critical step toward adaptive tools for managing evolving pathogens.

Conclusion

This study advances HIV/AIDS modeling through a fractal-fractional framework, integrating Atangana-Baleanu-Caputo (ABC) operators to better capture memory-driven transmission dynamics and spatial heterogeneity. We first validated the model's core properties-ensuring solution positivity, equilibrium existence, and stability-laying a rigorous foundation for epidemiological relevance. Stability analysis confirmed that the disease-free equilibrium remains both locally and globally stable when the basic reproduction number $\mathscr{R}_0 < 1$, aligning with real-world observations where effective control measures (e.g., early ART initiation) suppress outbreaks. Numerical simulations revealed how fractional-fractal orders (FFOs) and parameters shape transmission: lower FFOs amplify historical dependencies, mimicking delayed intervention effects, while higher FFOs smooth trajectories, reflecting rapid treatment scaling. The proposed Adam-Bashforth-form iterative method has proved to be a critical advancement, enabling highly accurate simulations of the intricate dynamics between susceptible, infected, treated, and AIDS-stage populations. In the identification of traditional fractal models and fractional calculus, this paradigm provides an enhanced model for modeling nonlinear processes such as drug resistance and involving immunity-sub domains in which conventional integer-order models often fail. Future research may extend this method to populations with spatial organization or include random components for handling randomness in super-spreading events. Verification by locally controlled HIV incidence rates would more completely confirm predictive ability, leading theoretical development toward informative applications to public health. As a concluding analysis, fractal-fractional calculus represents a transformative approach to infectious disease modeling, emphasizing adaptability and biological realism. Its capacity to incorporate memory effects and spatial complexity establishes it as an essential tool for developing dynamics strategies to combat evolving pathogens, form HIV to emerging pandemic.

Data availability

All data used is included in the paper.

Received: 9 January 2025; Accepted: 6 March 2025
Published online: 18 March 2025

References

1. Van Schalkwyk, C., Mahy, M., Johnson, L. F. & Imai-Eaton, J. W. Updated data and methods for the 2023 unaids hiv estimates. *Sci Rep* **95**, e1–e4 (2024).
2. Payagala, S. & Pozniak, A. The global burden of hiv. *Sci Rep* **42**, 119–127 (2024).

3. Ghazy, R. M., Al Awaidy, S. & Taha, S. H. N. Trends of hiv indicators in egypt from 1990 to 2021: time-series analysis and forecast toward unaids 90–90-90 targets. *BMC Public Health* **23**, 625 (2023).
4. Coleman, R. Setting the scene, setting the targets. the joint united nations programme on hiv/aids prevention targets of 2016 and estimating global pre-exposure prophylaxis targets. *Sex. Health* **15**, 485–488 (2018).
5. Phillips, J. A. Hiv and workers. *Workplace Health Saf.* **69**, 541 (2021).
6. Satoh, S. & Boyer, E. Hiv in south africa. *Lancet* **394**, 467 (2019).
7. Wang, X., Liu, X., Xu, W. & Zhang, K. Stochastic dynamics of hiv models with switching parameters and pulse control. *J. Frankl. Inst.* **352**, 2765–2782 (2015).
8. Bachar, M. & Dorfmayr, A. Hiv treatment models with time delay. *C. R. Biol.* **327**, 983–994 (2004).
9. Huo, H.-F. & Feng, L.-X. Global stability for an hiv/aids epidemic model with different latent stages and treatment. *Appl. Math. Model.* **37**, 1480–1489 (2013).
10. Djilali, S. Generalities on a delayed spatiotemporal host-pathogen infection model with distinct dispersal rates. *Math. Model. Nat. Phenom.* **19**, 11 (2024).
11. Xu, B., Li, J. & Wang, M. Epidemiological and time series analysis on the incidence and death of aids and hiv in china. *BMC Public Health* **20**, 1–10 (2020).
12. Heath, K., Levi, J. & Hill, A. The joint united nations programme on hiv/aids 95–95-95 targets: worldwide clinical and cost benefits of generic manufacture. *AIDS* **35**, S197–S203 (2021).
13. Gupta, P. K. & Dutta, A. A mathematical model on hiv/aids with fusion effect: Analysis and homotopy solution. *Eur. Phys. J. Plus* **134**, 265 (2019).
14. Teklu, S. W. & Rao, K. P. Hiv/aids-pneumonia codynamics model analysis with vaccination and treatment. *Comput. Math. Methods Med.* **2022**, 3105734 (2022).
15. Hogan, J. W., Galai, N. & Davis, W. W. Modeling the impact of social determinants of health on hiv. *AIDS Behav.* **25**, 215–224 (2021).
16. Legese, H., Degefa, H., Gebrewahd, A. & Gebremedhin, H. Utilization of isoniazid prophylaxis therapy and its associated factors among hiv positive clients taking antiretroviral therapy at fre semaetat primary hospital, hawzien districts, tigrai, northern ethiopia. *Trop. Dis. Travel Med. Vaccines* **6**, 1–7 (2020).
17. Johnson, M. The hiv epidemic and the covid-19 pandemic: Conversations with lgbtq+ elders of color on two public health crises. *J. Black Sex. Relat.* **8**, 23–46 (2022).
18. Makau, K. A. *Modling HIV AIDS dynamic with funding along the northern corridor highwat in kenya*. Ph.D. thesis, Kenyatta Univ. (2023).
19. Hasib, K., Jehad, A., K., A. D. & Khalaf, A. W. The use of artificial intelligence in data analysis with error recognitions in liver transplantation in hiv-aids patients using modified abc fractional order operators. *Fractal & Fractional* **9**, 16 (2025).
20. Mochan, E. & Sego, T. Mathematical modeling of the lethal synergism of coinfecting pathogens in respiratory viral infections: A review. *Microorganisms* **11**, 2974 (2023).
21. Rodrigo, C. & Rajapakse, S. Current status of hiv/aids in south asia. *J. Glob. Infect. Dis.* **1**, 93–101 (2009).
22. Perelson, A. S. & Nelson, P. W. Mathematical analysis of hiv-1 dynamics in vivo. *SIAM Rev.* **41**, 3–44 (1999).
23. Cui, Q. et al. Bifurcation and controller design of 5d bam neural networks with time delay. *Int. J. Numer. Model. Electron. Netw. Devices Fields* **37**, e3316 (2024).
24. Djilali, S., Chen, Y. & Bentout, S. Dynamics of a delayed nonlocal reaction-diffusion heroin epidemic model in a heterogenous environment. *Math. Methods Appl. Sci.* **48**, 273–307 (2025).
25. Djilali, S. Dynamics of a spatiotemporal sis epidemic model with distinct mobility range. *Appl. Anal.* 1–23 (2024).
26. Hasib, K. et al. On fractal-fractional waterborne disease model: A study on theoretical and numerical aspects of solutions via simulations. *Fractals* **34**, 2340055 (2023).
27. Atangana, A. & Baleanu, D. New fractional derivatives with nonlocal and non-singular kernel: theory and application to heat transfer model. arXiv preprint arXiv:1602.03408 (2016).
28. Khan, N., Ali, A., Ullah, A. & Khan, Z. A. Mathematical analysis of neurological disorder under fractional order derivative. *AIMS Math.* **8**, 18846–18865 (2023).
29. Ghanbari, B. & Atangana, A. A new application of fractional atangana-baleanu derivatives: designing abc-fractional masks in image processing. *Physica A* **542**, 123516 (2020).
30. Xu, C. *et al.* Mathematical analysis and dynamical transmission of (seirisr) model with different infection stages by using fractional operator. *Int. J. Biomathematics* (2024).
31. Xu, C., Farman, M. & Shehzad, A. Analysis and chaotic behavior of a fish farming model with singular and non-singular kernel. *Int. J. Biomathematics* 2350105 (2023).
32. Shukla, V. K., Joshi, M. C., Mishra, P. K. & Xu, C. Adaptive fixed-time difference synchronization for different classes of chaotic dynamical systems. *Phys. Scr.* **99**, 095264 (2024).
33. Hasib, K., jehad, A., Gomez-Aguilar & Praveen., A. Piecewise mabc fractional derivative with an application. *AIMS Mathematics* **8**, 24345–24366 (2023).
34. Atangana, A. & Qureshi, S. Modeling attractors of chaotic dynamical systems with fractal-fractional operators. *Chaos Solitons Fractals* **123**, 320–337 (2019).
35. Hogan, A. B. et al. Potential impact of the covid-19 pandemic on hiv, tuberculosis, and malaria in low-income and middle-income countries: a modelling study. *Lancet Glob. Health* **8**, e1132–e1141 (2020).
36. Abdeljawad, T. Fractional operators with generalized mittag-leffler kernels and their iterated differintegrals. *Chaos* **29** (2019).
37. Shah, K., Abdalla, B., Abdeljawad, T. & Alqudah, M. A. A fractal-fractional order model to study multiple sclerosis: a chronic disease. *Fractals* **32**, 2440010 (2024).
38. Baber, M. Z., Yasin, M. W., Xu, C., Ahmed, N. & Iqbal, M. S. Numerical and analytical study for the stochastic spatial dependent prey–predator dynamical system. *J. Comput. Nonlinear Dyn.* **19** (2024).
39. Eaton, J. W. et al. Health benefits, costs, and cost-effectiveness of earlier eligibility for adult antiretroviral therapy and expanded treatment coverage: a combined analysis of 12 mathematical models. *Lancet Glob. Health* **2**, e23–e34 (2014).
40. Diekmann, O., Heesterbeek, H. & Britton, T. *Mathematical tools for understanding infectious disease dynamics* Vol. 7 (Springer, 2013).
41. Naik, P. A., Yavuz, M., Qureshi, S., Zu, J. & Townley, S. Modeling and analysis of covid-19 epidemics with treatment in fractional derivatives using real data from pakistan. *Eur. Phys. J. Plus* **135**, 1–42 (2020).
42. De Cao, E., Zagheni, E., Manfredi, P. & Melegaro, A. The relative importance of frequency of contacts and duration of exposure for the spread of directly transmitted infections. *Biostat.* **15**, 470–483 (2014).
43. Yavuz, M. & Sene, N. Stability analysis and numerical computation of the fractional predator-prey model with the harvesting rate. *Fractal Fract.* **4**, 35 (2020).
44. Omame, A. *et al.* Understanding the impact of hiv on mpox transmission in an msm population: a mathematical modeling study. *Infect. Dis. Model.* (2024).
45. Ullah, M. A., Raza, N., Omame, A. & Alqarni, M. A new co-infection model for hbv and hiv with vaccination and asymptomatic transmission using actual data from taiwan. *Phys. Scr.* **99**, 065254 (2024).
46. Xu, C., Liao, M., Farman, M. & Shehzad, A. Hydrogenolysis of glycerol by heterogeneous catalysis: a fractional order kinetic model with analysis. *MATCH Commun. Math. Comput. Chem.* **91**, 635–664 (2024).

47. Xu, C., Farman, M., Shehzad, A. & Sooppy Nisar, K. Modeling and ulam–hyers stability analysis of oleic acid epoxidation by using a fractional-order kinetic model. *Math. Methods Appl. Sci.* (2024).
48. Farman, M. et al. Stability and chemical modeling of quantifying disparities in atmospheric analysis with sustainable fractal fractional approach. *Commun. Nonlinear Sci. Numer. Simul.* **142**, 108525 (2025).
49. Shah, K. & Abdeljawad, T. On complex fractal-fractional order mathematical modeling of co_2 emanations from energy sector. *Physica Scripta* **99**, 015226 (2023).
50. Khan, Z. A., Shah, K., Abdalla, B. & Abdeljawad, T. A numerical study of complex dynamics of a chemostat model under fractal-fractional derivative. *Fractals* **31**, 2340181 (2023).
51. Djilali, S., Sarmad, G. & Tridane, A. Dynamics and asymptotic profiles of a local-nonlocal dispersal sir epidemic model with spatial heterogeneity. *Infect. Dis. Model.* **10**, 387–409 (2025).
52. Odibat, Z. M. & Shawagfeh, N. T. Generalized taylor's formula. *Appl. Math. Comput.* **186**, 286–293 (2007).
53. Lin, J. et al. Bifurcation and controller design in a 3d delayed predator-prey model. *AIMS Math.* **9**, 33891–33929 (2024).
54. Lin, W. Global existence theory and chaos control of fractional differential equations. *J. Math. Anal. Appl.* **332**, 709–726 (2007).
55. Zhao, Y. et al. Mathematical exploration on control of bifurcation for a 3d predator-prey model with delay. *AIMS Math.* **9**, 29883–29915 (2024).
56. Johnson, A. T. *Biology for Engineers* (CRC Press, 2018).
57. Van den Driessche, P. & Watmough, J. Reproduction numbers and sub-threshold endemic equilibria for compartmental models of disease transmission. *Math. Biosci.* **180**, 29–48 (2002).
58. Chitnis, N., Hyman, J. M. & Cushing, J. M. Determining important parameters in the spread of malaria through the sensitivity analysis of a mathematical model. *Bull. Math. Biol.* **70**, 1272–1296 (2008).
59. Omame, A. et al. Dynamics of mpox in an hiv endemic community: A mathematical modelling approach. *Math. Biosci. Eng.* **22**, 225–259 (2025).
60. Castillo-Chavez, C. & Song, B. Dynamical models of tuberculosis and their applications. *Math. Biosci. Eng.* **1**, 361–404 (2004).
61. Chitnis, N., Cushing, J. M. & Hyman, J. Bifurcation analysis of a mathematical model for malaria transmission. *SIAM J. Appl. Math.* **67**, 24–45 (2006).
62. Djilali, S., Bentout, S. & Tridane, A. Dynamics of a generalized nonlocal dispersion sis epidemic model. *J. Evol. Equ.* **24**, 83 (2024).
63. Peinado, J., Ibáñez, J., Arias, E. & Hernández, V. Adams-bashforth and adams-moulton methods for solving differential riccati equations. *Comput. Math. Appl.* **60**, 3032–3045 (2010).
64. Li, B., Zhang, T. & Zhang, C. Investigation of financial bubble mathematical model under fractal-fractional caputo derivative. *Fractals* **31**, 2350050 (2023).
65. Rashid, S. et al. Robustness and exploration between the interplay of the nonlinear co-dynamics hiv/aids and pneumonia model via fractional differential operators and a probabilistic approach. *Sci. Rep.* **14**, 16922 (2024).
66. Zouari, F. Neural network based adaptive backstepping dynamic surface control of drug dosage regimens in cancer treatment. *Neurocomputing* **366**, 248–263 (2019).
67. Naik, P. A., Yeolekar, B. M., Qureshi, S., Yeolekar, M. & Madzvamuse, A. Modeling and analysis of the fractional-order epidemic model to investigate mutual influence in hiv/hcv co-infection. *Nonlinear Dyn.* 1–32 (2024).
68. Bentout, S. & Djilali, S. Asymptotic profiles of a generalized reaction-diffusion sis epidemic model with spatial heterogeneity. *Z. Angew. Math. Phys.* **75**, 1–31 (2024).
69. Gudaz, H., Ogu, H. A. & Schwartz, E. J. Long-term dynamics of the kidney disease epidemic among hiv-infected individuals. *Spora J. Biomathematics* **6**, 52–60 (2020).
70. McMahon, A. et al. Reinfection with sars-cov-2: Discrete sir (susceptible, infected, recovered) modeling using empirical infection data. *JMIR Public Health Surveill.* **6**, e21168 (2020).
71. Yaesoubi, R. & Cohen, T. Generalized markov models of infectious disease spread: A novel framework for developing dynamic health policies. *Eur. J. Oper. Res.* **215**, 679–687 (2011).
72. Zhang, W. *et al.* Behavior changes influence mpox transmission in the united states, 2022–2023: Insights from homogeneous and heterogeneous models. *PNAS Nexus* **4**, pgaf025 (2025).
73. Tang, L. et al. A review of multi-compartment infectious disease models. *Int. Stat. Rev.* **88**, 462–513 (2020).
74. Ijeh, S., Okolo, C. A., Arowoogun, J. O., Adeniyi, A. O. & Omotayo, O. Predictive modeling for disease outbreaks: a review of data sources and accuracy. *Int. Med. Sci. Res. J.* **4**, 406–419 (2024).

Acknowledgements
The authors express their gratitude to Prince Sultan University, Saudi Arabia, for APC and support of this work through TAS lab.

Author contributions
All authors reviewed and approved the final manuscript.

Funding
We are thankful to Prince Sultan University, Saudi Arabia, for funding this research.

Declarations

Competing interests
The authors declare no competing interests.

Additional information
Correspondence and requests for materials should be addressed to N.K. or T.A.